Physics Letters B 753 (2016) 629–638

Contents lists available at ScienceDirect

Physics Letters B

www.elsevier.com/locate/physletb

Measurement of the $e^+e^- \to \pi^+\pi^-$ cross section between 600 and 900 MeV using initial state radiation

BESIII Collaboration

M. Ablikim [a], M.N. Achasov [i,6], X.C. Ai [a], O. Albayrak [e], M. Albrecht [d], D.J. Ambrose [av], A. Amoroso [ba,bc], F.F. An [a], Q. An [ax,1], J.Z. Bai [a], R. Baldini Ferroli [t], Y. Ban [ag], D.W. Bennett [s], J.V. Bennett [e], M. Bertani [t], D. Bettoni [v], J.M. Bian [au], F. Bianchi [ba,bc], E. Boger [y,4], I. Boyko [y], R.A. Briere [e], H. Cai [be], X. Cai [a,1], O. Cakir [ap,2], A. Calcaterra [t], G.F. Cao [a], S.A. Cetin [aq], J.F. Chang [a,1], G. Chelkov [y,4,5], G. Chen [a], H.S. Chen [a], H.Y. Chen [b], J.C. Chen [a], M.L. Chen [a,1], S.J. Chen [ae], X. Chen [a,1], X.R. Chen [ab], Y.B. Chen [a,1], H.P. Cheng [q], X.K. Chu [ag], G. Cibinetto [v], H.L. Dai [a,1], J.P. Dai [aj], A. Dbeyssi [n], D. Dedovich [y], Z.Y. Deng [a], A. Denig [x,*], I. Denysenko [y], M. Destefanis [ba,bc], F. De Mori [ba,bc], Y. Ding [ac], C. Dong [af], J. Dong [a,1], L.Y. Dong [a], M.Y. Dong [a,1], S.X. Du [bg], P.F. Duan [a], E.E. Eren [aq], J.Z. Fan [ao], J. Fang [a,1], S.S. Fang [a], X. Fang [ax,1], Y. Fang [a], L. Fava [bb,bc], F. Feldbauer [x], G. Felici [t], C.Q. Feng [ax,1], E. Fioravanti [v], M. Fritsch [n,x], C.D. Fu [a], Q. Gao [a], X.Y. Gao [b], Y. Gao [ao], Z. Gao [ax,1], I. Garzia [v], K. Goetzen [j], W.X. Gong [a,1], W. Gradl [x], M. Greco [ba,bc], M.H. Gu [a,1], Y.T. Gu [l], Y.H. Guan [a], A.Q. Guo [a], L.B. Guo [ad], Y. Guo [a], Y.P. Guo [x], Z. Haddadi [aa], A. Hafner [x], S. Han [be], X.Q. Hao [o], F.A. Harris [at], K.L. He [a], X.Q. He [aw], T. Held [d], Y.K. Heng [a,1], Z.L. Hou [a], C. Hu [ad], H.M. Hu [a], J.F. Hu [ba,bc], T. Hu [a,1], Y. Hu [a], G.M. Huang [f], G.S. Huang [ax,1], J.S. Huang [o], X.T. Huang [ai], Y. Huang [ae], T. Hussain [az], Q. Ji [a], Q.P. Ji [af], X.B. Ji [a], X.L. Ji [a,1], L.W. Jiang [be], X.S. Jiang [a,1], X.Y. Jiang [af], J.B. Jiao [ai], Z. Jiao [q], D.P. Jin [a,1], S. Jin [a], T. Johansson [bd], A. Julin [au], N. Kalantar-Nayestanaki [aa], X.L. Kang [a], X.S. Kang [af], M. Kavatsyuk [aa], B.C. Ke [e], P. Kiese [x], R. Kliemt [n], B. Kloss [x,*], O.B. Kolcu [aq,9], B. Kopf [d], M. Kornicer [at], W. Kühn [z], A. Kupsc [bd], J.S. Lange [z], M. Lara [s], P. Larin [n], C. Leng [bc], C. Li [bd], Cheng Li [ax,1], D.M. Li [bg], F. Li [a,1], F.Y. Li [ag], G. Li [a], H.B. Li [a], J.C. Li [a], Jin Li [ah], K. Li [ai], K. Li [m], Lei Li [c], P.R. Li [as], T. Li [ai], W.D. Li [a], W.G. Li [a], X.L. Li [ai], X.M. Li [l], X.N. Li [a,1], X.Q. Li [af], Z.B. Li [an], H. Liang [ax,1], Y.F. Liang [al], Y.T. Liang [z], G.R. Liao [k], D.X. Lin [n], B.J. Liu [a], C.X. Liu [a], F.H. Liu [ak], Fang Liu [a], Feng Liu [f], H.B. Liu [l], H.H. Liu [p], H.H. Liu [a], H.M. Liu [a], J. Liu [a], J.B. Liu [ax,1], J.P. Liu [be], J.Y. Liu [a], K. Liu [ao], K.Y. Liu [ac], L.D. Liu [ag], P.L. Liu [a,1], Q. Liu [as], S.B. Liu [ax,1], X. Liu [ab], Y.B. Liu [af], Z.A. Liu [a,1], Zhiqing Liu [x], H. Loehner [aa], X.C. Lou [a,1,8], H.J. Lu [q], J.G. Lu [a,1], Y. Lu [a], Y.P. Lu [a,1], C.L. Luo [ad], M.X. Luo [bf], T. Luo [at], X.L. Luo [a,1], X.R. Lyu [as], F.C. Ma [ac], H.L. Ma [a], L.L. Ma [ai], Q.M. Ma [a], T. Ma [a], X.N. Ma [af], X.Y. Ma [a,1], F.E. Maas [n], M. Maggiora [ba,bc], Y.J. Mao [ag], Z.P. Mao [a], S. Marcello [ba,bc], J.G. Messchendorp [aa], J. Min [a,1], R.E. Mitchell [s], X.H. Mo [a,1], Y.J. Mo [f], C. Morales Morales [n], K. Moriya [s], N.Yu. Muchnoi [i,6], H. Muramatsu [au], Y. Nefedov [y], F. Nerling [n], I.B. Nikolaev [i,6], Z. Ning [a,1], S. Nisar [h], S.L. Niu [a,1], X.Y. Niu [a], S.L. Olsen [ah], Q. Ouyang [a,1], S. Pacetti [u], P. Patteri [t], M. Pelizaeus [d], H.P. Peng [ax,1], K. Peters [j], J. Pettersson [bd], J.L. Ping [ad], R.G. Ping [a], R. Poling [au], V. Prasad [a], M. Qi [ae], S. Qian [a,1], C.F. Qiao [as], L.Q. Qin [ai], N. Qin [be], X.S. Qin [a], Z.H. Qin [a,1], J.F. Qiu [a], K.H. Rashid [az], C.F. Redmer [x], M. Ripka [x], G. Rong [a], Ch. Rosner [n], X.D. Ruan [l], V. Santoro [v], A. Sarantsev [y,7], M. Savrié [w], K. Schoenning [bd], S. Schumann [x], W. Shan [ag], M. Shao [ax,1], C.P. Shen [b], P.X. Shen [af], X.Y. Shen [a], H.Y. Sheng [a], W.M. Song [a],

http://dx.doi.org/10.1016/j.physletb.2015.11.043

M.R. Shepherd [s], X.Y. Song [a], S. Sosio [ba,bc], S. Spataro [ba,bc], G.X. Sun [a], J.F. Sun [o], S.S. Sun [a], Y.J. Sun [ax,1], Y.Z. Sun [a], Z.J. Sun [a,1], Z.T. Sun [s], C.J. Tang [al], X. Tang [a], I. Tapan [ar], E.H. Thorndike [av], M. Tiemens [aa], M. Ullrich [z], I. Uman [aq], G.S. Varner [at], B. Wang [af], D. Wang [ag], D.Y. Wang [ag], K. Wang [a,1], L.L. Wang [a], L.S. Wang [a], M. Wang [ai], P. Wang [a], P.L. Wang [a], S.G. Wang [ag], W. Wang [a,1], X.F. Wang [ao], Y.D. Wang [n], Y.F. Wang [a,1], Y.Q. Wang [x], Z. Wang [a,1], Z.G. Wang [a,1], Z.H. Wang [ax,1], Z.Y. Wang [a], T. Weber [x], D.H. Wei [k], J.B. Wei [ag], P. Weidenkaff [x], S.P. Wen [a], U. Wiedner [d], M. Wolke [bd], L.H. Wu [a], Z. Wu [a,1], L.G. Xia [ao], Y. Xia [r], D. Xiao [a], H. Xiao [ay], Z.J. Xiao [ad], Y.G. Xie [a,1], Q.L. Xiu [a,1], G.F. Xu [a], L. Xu [a], Q.J. Xu [m], X.P. Xu [am], L. Yan [ax,1], W.B. Yan [ax,1], W.C. Yan [ax,1], Y.H. Yan [r], H.J. Yang [aj], H.X. Yang [a], L. Yang [be], Y. Yang [f], Y.X. Yang [k], M. Ye [a,1], M.H. Ye [g], J.H. Yin [a], B.X. Yu [a,1], C.X. Yu [af], J.S. Yu [ab], C.Z. Yuan [a], W.L. Yuan [ae], Y. Yuan [a], A. Yuncu [aq,3], A.A. Zafar [az], A. Zallo [t], Y. Zeng [r], B.X. Zhang [a], B.Y. Zhang [a,1], C. Zhang [ae], C.C. Zhang [a], D.H. Zhang [a], H.H. Zhang [an], H.Y. Zhang [a,1], J.J. Zhang [a], J.L. Zhang [a], J.Q. Zhang [a], J.W. Zhang [a,1], J.Y. Zhang [a], J.Z. Zhang [a], K. Zhang [a], L. Zhang [a], X.Y. Zhang [ai], Y. Zhang [a], Y.N. Zhang [as], Y.H. Zhang [a,1], Y.T. Zhang [ax,1], Yu Zhang [as], Z.H. Zhang [f], Z.P. Zhang [ax], Z.Y. Zhang [be], G. Zhao [a], J.W. Zhao [a,1], J.Y. Zhao [a], J.Z. Zhao [a,1], Lei Zhao [ax,1], Ling Zhao [a], M.G. Zhao [af], Q. Zhao [a], Q.W. Zhao [a], S.J. Zhao [bg], T.C. Zhao [a], Y.B. Zhao [a,1], Z.G. Zhao [ax,1], A. Zhemchugov [y,4], B. Zheng [ay], J.P. Zheng [a,1], W.J. Zheng [ai], Y.H. Zheng [as], B. Zhong [ad], L. Zhou [a,1], X. Zhou [be], X.K. Zhou [ax,1], X.R. Zhou [ax,1], X.Y. Zhou [a], K. Zhu [a], K.J. Zhu [a,1], S. Zhu [a], S.H. Zhu [aw], X.L. Zhu [ao], Y.C. Zhu [ax,1], Y.S. Zhu [a], Z.A. Zhu [a], J. Zhuang [a,1], L. Zotti [ba,bc], B.S. Zou [a], J.H. Zou [a]

[a] *Institute of High Energy Physics, Beijing 100049, People's Republic of China*
[b] *Beihang University, Beijing 100191, People's Republic of China*
[c] *Beijing Institute of Petrochemical Technology, Beijing 102617, People's Republic of China*
[d] *Bochum Ruhr-University, D-44780 Bochum, Germany*
[e] *Carnegie Mellon University, Pittsburgh, PA 15213, USA*
[f] *Central China Normal University, Wuhan 430079, People's Republic of China*
[g] *China Center of Advanced Science and Technology, Beijing 100190, People's Republic of China*
[h] *COMSATS Institute of Information Technology, Lahore, Defence Road, Off Raiwind Road, 54000 Lahore, Pakistan*
[i] *G.I. Budker Institute of Nuclear Physics SB RAS (BINP), Novosibirsk 630090, Russia*
[j] *GSI Helmholtzcentre for Heavy Ion Research GmbH, D-64291 Darmstadt, Germany*
[k] *Guangxi Normal University, Guilin 541004, People's Republic of China*
[l] *GuangXi University, Nanning 530004, People's Republic of China*
[m] *Hangzhou Normal University, Hangzhou 310036, People's Republic of China*
[n] *Helmholtz Institute Mainz, Johann-Joachim-Becher-Weg 45, D-55099 Mainz, Germany*
[o] *Henan Normal University, Xinxiang 453007, People's Republic of China*
[p] *Henan University of Science and Technology, Luoyang 471003, People's Republic of China*
[q] *Huangshan College, Huangshan 245000, People's Republic of China*
[r] *Hunan University, Changsha 410082, People's Republic of China*
[s] *Indiana University, Bloomington, IN 47405, USA*
[t] *INFN Laboratori Nazionali di Frascati, I-00044, Frascati, Italy*
[u] *INFN and University of Perugia, I-06100, Perugia, Italy*
[v] *INFN Sezione di Ferrara, I-44122, Ferrara, Italy*
[w] *University of Ferrara, I-44122, Ferrara, Italy*
[x] *Johannes Gutenberg University of Mainz, Johann-Joachim-Becher-Weg 45, D-55099 Mainz, Germany*
[y] *Joint Institute for Nuclear Research, 141980 Dubna, Moscow region, Russia*
[z] *Justus Liebig University Giessen, II. Physikalisches Institut, Heinrich-Buff-Ring 16, D-35392 Giessen, Germany*
[aa] *KVI-CART, University of Groningen, NL-9747 AA Groningen, The Netherlands*
[ab] *Lanzhou University, Lanzhou 730000, People's Republic of China*
[ac] *Liaoning University, Shenyang 110036, People's Republic of China*
[ad] *Nanjing Normal University, Nanjing 210023, People's Republic of China*
[ae] *Nanjing University, Nanjing 210093, People's Republic of China*
[af] *Nankai University, Tianjin 300071, People's Republic of China*
[ag] *Peking University, Beijing 100871, People's Republic of China*
[ah] *Seoul National University, Seoul, 151-747, Republic of Korea*
[ai] *Shandong University, Jinan 250100, People's Republic of China*
[aj] *Shanghai Jiao Tong University, Shanghai 200240, People's Republic of China*
[ak] *Shanxi University, Taiyuan 030006, People's Republic of China*
[al] *Sichuan University, Chengdu 610064, People's Republic of China*
[am] *Soochow University, Suzhou 215006, People's Republic of China*
[an] *Sun Yat-Sen University, Guangzhou 510275, People's Republic of China*
[ao] *Tsinghua University, Beijing 100084, People's Republic of China*
[ap] *Istanbul Aydin University, 34295 Sefakoy, Istanbul, Turkey*
[aq] *Dogus University, 34722 Istanbul, Turkey*
[ar] *Uludag University, 16059 Bursa, Turkey*
[as] *University of Chinese Academy of Sciences, Beijing 100049, People's Republic of China*
[at] *University of Hawaii, Honolulu, HI 96822, USA*
[au] *University of Minnesota, Minneapolis, MN 55455, USA*
[av] *University of Rochester, Rochester, NY 14627, USA*

[aw] University of Science and Technology Liaoning, Anshan 114051, People's Republic of China
[ax] University of Science and Technology of China, Hefei 230026, People's Republic of China
[ay] University of South China, Hengyang 421001, People's Republic of China
[az] University of the Punjab, Lahore-54590, Pakistan
[ba] University of Turin, I-10125, Turin, Italy
[bb] University of Eastern Piedmont, I-15121, Alessandria, Italy
[bc] INFN, I-10125, Turin, Italy
[bd] Uppsala University, Box 516, SE-75120 Uppsala, Sweden
[be] Wuhan University, Wuhan 430072, People's Republic of China
[bf] Zhejiang University, Hangzhou 310027, People's Republic of China
[bg] Zhengzhou University, Zhengzhou 450001, People's Republic of China

ARTICLE INFO

Article history:
Received 30 July 2015
Received in revised form 28 October 2015
Accepted 14 November 2015
Available online 28 November 2015
Editor: V. Metag

Keywords:
Hadronic cross section
Muon anomaly
Initial state radiation
Pion form factor
BESIII

ABSTRACT

We extract the $e^+e^- \to \pi^+\pi^-$ cross section in the energy range between 600 and 900 MeV, exploiting the method of initial state radiation. A data set with an integrated luminosity of 2.93 fb^{-1} taken at a center-of-mass energy of 3.773 GeV with the BESIII detector at the BEPCII collider is used. The cross section is measured with a systematic uncertainty of 0.9%. We extract the pion form factor $|F_\pi|^2$ as well as the contribution of the measured cross section to the leading-order hadronic vacuum polarization contribution to $(g-2)_\mu$. We find this value to be $a_\mu^{\pi\pi,\mathrm{LO}}(600\text{–}900\ \mathrm{MeV}) = (368.2 \pm 2.5_{\mathrm{stat}} \pm 3.3_{\mathrm{sys}}) \cdot 10^{-10}$, which is between the corresponding values using the BaBar or KLOE data.

1. Introduction

The cross section $\sigma_{\pi\pi} = \sigma(e^+e^- \to \pi^+\pi^-)$ has been measured in the past with ever increasing precision at accelerators in Novosibirsk [1–3], Orsay [4], Frascati [5–8], and SLAC [9,10]. More recently, the two most precise measurements have been performed by the KLOE Collaboration in Frascati [8] and the BaBar Collaboration at SLAC [9,10]. Both experiments claim a precision of better than 1% in the energy range below 1 GeV, in which the $\rho(770)$ resonance with its decay into pions dominates the total hadronic cross section. A discrepancy of approximately 3% on the peak of the $\rho(770)$ resonance is observed between the KLOE and BaBar spectra. The discrepancy is even increasing towards higher energies above the peak of the ρ resonance. Unfortunately, this discrepancy is limiting the current knowledge of the anomalous magnetic moment of the muon $a_\mu \equiv (g-2)_\mu/2$ [11], a precision observable of the Standard Model (SM). The accuracy of the SM prediction of $(g-2)_\mu$ is entirely limited by the knowledge of the hadronic vacuum polarization contribution, which is obtained in a dispersive framework by using experimental data on $\sigma(e^+e^- \to \text{hadrons})$ [11–13]. The cross section $\sigma(e^+e^- \to \pi^+\pi^-)$ contributes to more than 70% to this dispersion relation and, hence, is the most important exclusive hadronic channel of the total hadronic cross section. Currently, a discrepancy of 3.6 standard deviations [12] is found between the direct measurement of a_μ and its SM prediction. However, the discrepancy reduces to 2.4σ [14], when only BaBar data is used as input to the dispersion relation. In this letter we present a new measurement of the cross section $\sigma_{\pi\pi}$, obtained by the BESIII experiment at the BEPCII collider in Beijing.

The measurement exploits the method of initial state radiation (ISR), the same method as used by BaBar and KLOE. In the ISR method events are used in which one of the beam particles radiates a high-energy photon. In such a way, the available energy to produce a hadronic (or leptonic) final state is reduced, and the hadronic (or leptonic) mass range below the center-of-mass (cms) energy of the e^+e^- collider becomes available. In this paper, we restrict the studies to the mass range between 600 and 900 MeV/c^2, which corresponds to the ρ peak region.

The remainder of this letter is organized as follows: In section 2, the BESIII experiment is introduced. In section 3 we describe the data set used, the Monte Carlo (MC) simulation, the event selection of $e^+e^- \to \pi^+\pi^-\gamma$ events, and the data-MC efficiency corrections. The determination of the integrated luminosity of the data set is described in Section 4. A cross check of the used efficiency corrections using the well-known $e^+e^- \to \mu^+\mu^-\gamma$ QED process is performed in Section 5, before extracting the $\pi^+\pi^-$ cross section in Section 6.

2. The BESIII experiment

The BESIII detector is located at the double-ring Beijing electron–positron collider (BEPCII) [15].

The cylindrical BESIII detector covers 93% of the full solid angle. It consists of the following detector systems. (1) A Multilayer Drift Chamber (MDC), filled with helium gas, composed of 43 layers, which provides a spatial resolution of 135 µm, an ionization energy loss dE/dx resolution better than 6%, and a momentum resolution of 0.5% for charged tracks at 1 GeV/c. (2) A Time-of-Flight system (TOF), built with 176 plastic scintillator counters in the barrel part, and 96 counters in the endcaps. The time resolution is 80 ps in the barrel and 110 ps in the endcaps. For momenta

* Corresponding author.
E-mail addresses: denig@kph.uni-mainz.de (A. Denig), kloss@uni-mainz.de (B. Kloss), liu@kph.uni-mainz.de (Z. Liu).

[1] Also at State Key Laboratory of Particle Detection and Electronics, Beijing 100049, Hefei 230026, People's Republic of China.
[2] Also at Ankara University, 06100 Tandogan, Ankara, Turkey.
[3] Also at Bogazici University, 34342 Istanbul, Turkey.
[4] Also at the Moscow Institute of Physics and Technology, Moscow 141700, Russia.
[5] Also at the Functional Electronics Laboratory, Tomsk State University, Tomsk, 634050, Russia.
[6] Also at the Novosibirsk State University, Novosibirsk, 630090, Russia.
[7] Also at the NRC "Kurchatov Institute", PNPI, 188300, Gatchina, Russia.
[8] Also at the University of Texas at Dallas, Richardson, Texas 75083, USA.
[9] Also at Istanbul Arel University, 34295 Istanbul, Turkey.

up to 1 GeV/c, this provides a 2σ K/π separation. (3) A CsI(Tl) Electro-Magnetic Calorimeter (EMC), with an energy resolution of 2.5% in the barrel and 5% in the endcaps at an energy of 1 GeV. (4) A superconducting magnet producing a magnetic field of 1T. (5) A Muon Chamber (MUC) consisting of nine barrel and eight endcap resistive plate chamber layers with a 2 cm position resolution.

3. Data sample, event selection, and efficiency corrections

3.1. Data sample and MC simulations

We analyze 2.93 fb^{-1} (see Sect. 4) of data taken at a cms energy $\sqrt{s} = 3.773$ GeV, which were collected in two separate runs in 2010 and 2011. The Phokhara event generator [16,17] is used to simulate the signal process $e^+e^- \to \pi^+\pi^-\gamma$ and the dominant background channel $\mu^+\mu^-\gamma$. The generator includes ISR and final state radiation (FSR) corrections up to next-to-leading order (NLO). Effects of ISR–FSR interference are included as well. The continuum $q\bar{q}$ ($q = u, d, s$) MC sample is produced with the KKMC event generator [18]. Bhabha scattering events are simulated with BABAYAGA 3.5 [19]. The Bhabha process is also used for the luminosity measurement. All MC generators have been interfaced with the GEANT4-based detector simulation [20,21].

3.2. Event selection

Events of the type $e^+e^- \to \pi^+\pi^-\gamma$ are selected. Only a tagged ISR analysis is possible in the mass range $600 < m_{\pi\pi} < 900$ MeV/c^2, where $m_{\pi\pi}$ is the $\pi^+\pi^-$ invariant mass, *i.e.*, the radiated photon has to be explicitly detected in the detector. For untagged events, the photon escapes detection along the beam pipe; the hadronic system recoiling against the ISR photon is therefore also strongly boosted towards small polar angles, resulting in no geometrical acceptance in the investigated $m_{\pi\pi}$ range.

We require the presence of two charged tracks in the MDC with net charge zero. The points of closest approach to the interaction point (IP) of both tracks have to be within a cylinder with 1 cm radius in the transverse direction and ± 10 cm of length along the beam axis. For three-track events, we choose the combination with net charge zero for which the tracks are closest to the IP. The polar angle θ of the tracks is required to be found in the fiducial volume of the MDC, 0.4 rad $< \theta < \pi - 0.4$ rad, where θ is the polar angle of the track with respect to the beam axis. We require the transverse momentum p_t to be above 300 MeV/c for each track. In addition, we require the presence of at least one neutral cluster in the EMC without associated hits in the MDC. We require a deposited energy above 400 MeV. This cluster is then treated as the ISR photon candidate.

The radiative Bhabha process $e^+e^- \to e^+e^-\gamma(\gamma)$ has a cross section which is up to three orders of magnitude larger than the signal cross section. Electron tracks, therefore, need to be suppressed. An electron particle identification (PID) algorithm is used for this purpose, exploiting information from the MDC, TOF and EMC [22]. The probabilities for being a pion $P(\pi)$ and being an electron $P(e)$ are calculated, and $P(\pi) > P(e)$ is required for both charged tracks.

Using as input the momenta of the two selected track candidates, the energy of the photon candidate, as well as the four-momentum of the initial e^+e^- system, a four-constraint (4C) kinematic fit enforcing energy and momentum conservation is performed which tests the hypothesis $e^+e^- \to \pi^+\pi^-\gamma$. Events are considered to match the hypothesis if they fulfill the requirement $\chi^2_{4C} < 60$. It turns out that the $\mu^+\mu^-\gamma$ final state cannot be suppressed by means of kinematic fitting due to the limited momentum resolution of the MDC. An independent separation of pion and muon tracks is required.

We utilize a track-based muon–pion separation, which is based on the Artificial Neural Network (ANN) method, as provided by the TMVA package [23]. The following observables are exploited for the separation: the Zernicke moments of the EMC clusters [22], induced by pion or muon tracks, the ratio of the energy E of a track deposited in the EMC and its momentum p measured in the MDC, the ionization energy loss dE/dx in the MDC, and the depth of a track in the MUC. The ANN is trained using $\pi^+\pi^-\gamma$ and $\mu^+\mu^-\gamma$ MC samples. We choose the implementation of a Clermont-Ferrand Multilayer Perceptron (CFMlp) ANN as the method resulting in the best background rejection for a given signal efficiency. The output likelihood $y_{\rm ANN}$ is calculated after training the ANN for the signal pion tracks and background muon tracks. The response value $y_{\rm ANN}$ is required to be greater than 0.6 for each pion candidate in the event selection, yielding a background rejection of more than 90% and a signal loss of less than 30%.

3.3. Efficiency corrections

Given the accuracy of $\mathcal{O}(1\%)$ targeted for the cross section measurement, possible discrepancies between data and MC due to imperfections of the detector simulation need to be considered. We have investigated data and MC distributions concerning the tracking performance, the energy measurement, and the PID probabilities, both for the electron PID as well as the pion–muon separation. In order to produce test samples of muon and pion tracks over a wide range in momentum/energy and polar angle, we select samples of $\mu^+\mu^-\gamma$ and $\pi^+\pi^-\pi^+\pi^-\gamma$ events that have impurities at the per mille level. By comparing the efficiencies found in data with the corresponding results found in the MC samples, we determine possible discrepancies. Corresponding correction factors are computed in bins of the track momentum or energy and the track polar angle θ, and are applied to MC tracks to adjust the reconstructed number of events. While for the reconstruction of charged tracks and neutral clusters and for electron PID, the differences between data and MC are smaller than 1% on average, differences up to 10% occur in the ANN case. The corrections are applied separately for neutral clusters and for muon and pion tracks. Hence, we do not only obtain the corrections for the $\pi^+\pi^-\gamma$ signal events, but also for the dominating $\mu^+\mu^-\gamma$ background. The statistical errors of the correction factors are included in the statistical uncertainty of the measurement. Systematic uncertainties associated to the correction factors are presented in Sect. 6.5. The efficiency correction for the photon efficiency is obtained after the application of the kinematic fit procedure. The corresponding correction is therefore a combined correction of photon efficiency and differences between data and MC of the χ^2_{4C} distribution. The systematic uncertainty for the contribution of the photon efficiency and χ^2_{4C} distribution is, hence, incorporated in the systematic effects associated with the efficiency corrections. The systematic uncertainty connected with the p_t requirement is also associated with the corresponding efficiency correction.

3.4. Background subtraction

The $\mu^+\mu^-\gamma$ background remaining after the application of the ANN is still of the order of a few percent, compared to 5×10^5 signal events. It is, however, known with high accuracy, as will be shown in the next section, and is subtracted based on MC simulation. Additional background beyond $\mu^+\mu^-\gamma$ remains below the one per mille level. Table 1 lists the remaining MC events after applying all requirements and scaling to the luminosity of the used data set.

Table 1
Total number of remaining non-muon background events between $600 < m_{\pi\pi} < 900$ MeV/c^2 obtained with MC samples.

Final state	Background events
$e^+e^-(n\gamma)$	12.0 ± 3.5
$\pi^+\pi^-\pi^0\gamma$	3.3 ± 1.8
$\pi^+\pi^-\pi^0\pi^0\gamma$	negl.
$K^+K^-\gamma$	2.0 ± 1.5
$K^0\overline{K^0}\gamma$	0.4 ± 0.6
$p\bar{p}\gamma$	negl.
continuum	3.9 ± 1.9
$\psi(3770) \to D^+D^-$	negl.
$\psi(3770) \to D^0\overline{D^0}$	negl.
$\psi(3770) \to$ non $D\overline{D}$	3.1 ± 1.8
$\gamma\ \psi(2S)$	negl.
$\gamma\ J/\psi$	0.6 ± 0.8

4. Luminosity measurement using Bhabha events

The integrated luminosity of the data set used in this work was previously measured in Ref. [24] with a precision of 1.0% using Bhabha scattering events. In the course of this analysis, we remeasure the luminosity and decrease its systematic uncertainty by the following means: (1) Usage of the BABAYAGA@NLO [25] event generator with a theoretical uncertainty of 0.1%, instead of the previously used BABAYAGA 3.5 event generator with an uncertainty of 0.5% [19]. (2) Precise estimation of the signal selection efficiencies. In particular, the uncertainty estimate of the polar angle acceptance is evaluated by data-MC studies within the fiducial EMC detection volume, which is relevant for the luminosity study (0.13%). The very conservative estimate in [24] was based on acceptance comparisons with and without using the transition region between the EMC barrel and endcaps, leading to additional data-MC differences (0.75%). The other uncertainties of [24] remain unchanged and additional systematic uncertainties due to the uncertainty of $\sqrt{s}$ (0.2%) and the vacuum polarization correction ($< 0.01\%$) are taken into account. Finally, the total integrated luminosity amounts to $\mathcal{L} = (2931.8 \pm 0.2_{\rm stat} \pm 13.8_{\rm sys})$ pb^{-1} with a relative uncertainty of 0.5%, which is consistent with the previous measurement [24].

5. QED test using $e^+e^- \to \mu^+\mu^-\gamma$ events

The yield of events of the channel $e^+e^- \to \mu^+\mu^-\gamma$ as a function of the two-muon invariant mass $m_{\mu\mu}$ can be compared to a precise prediction by QED, which is provided by the Phokhara generator. We select muon events according to the ANN method described previously and require $y_{\rm ANN} < 0.4$ for both tracks, resulting in a background rejection of more than 90% and a signal loss of less than 20%. All other requirements in the selection are exactly the same as for the $\pi^+\pi^-\gamma$ analysis. The remaining pion background after the $\mu^+\mu^-\gamma$ selection is much reduced, reaching 10% in the ρ peak region. A comparison between data and MC is shown in Fig. 1. The same data sample as used in the main analysis is also used here, but we present a larger mass range than for the $\pi^+\pi^-\gamma$ case. The efficiency corrections described in the previous section have been applied to MC on a track and photon candidate basis. The lower panel of Fig. 1 shows the relative discrepancy between data and MC. A good agreement over the full $m_{\mu\mu}$ mass range at the level of $(1.0 \pm 0.3 \pm 0.9)\%$ and $\chi^2/{\rm ndf} = 134/139$ is found, where the uncertainties are statistical and systematic, respectively. A difference in the mass resolution due to detector effects between data and MC is visible around the narrow J/ψ resonance. A fit in the mass range $600 < m_{\mu\mu} < 900$ MeV/c^2, which is the mass range studied in the main analysis, gives a relative discrepancy of $(2.0 \pm 1.7 \pm 0.9)\%$; this is illustrated in the inset of the upper panel of Fig. 1. The theoretical uncertainty of the MC

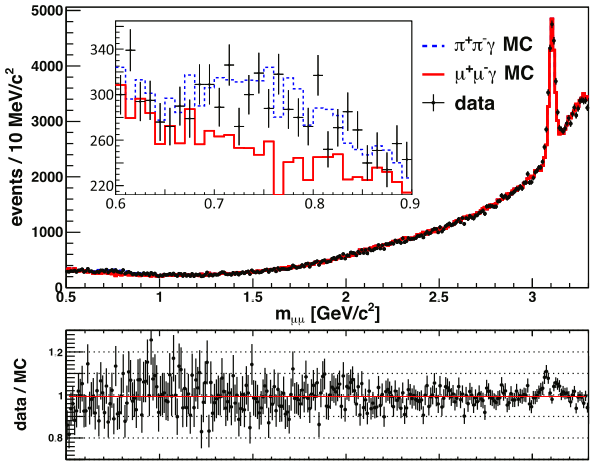

Fig. 1. Invariant $\mu^+\mu^-$ mass spectrum of data and $\mu^+\mu^-\gamma$ MC after using the ANN as muon selector and applying the efficiency corrections. The upper panel presents the absolute comparison of the number of events found in data and MC. The inset shows the zoom for invariant masses between 0.6 and 0.9 GeV/c^2. The MC sample is scaled to the luminosity of the data set. The lower plot shows the ratio of these two histograms. A linear fit is performed to quantify the data-MC difference, which gives a difference of $(1.0 \pm 0.3 \pm 0.9)\%$. A difference in the mass resolution between data and MC is visible around the narrow J/ψ resonance.

generator Phokhara is below 0.5% [16], while the systematic uncertainty of our measurement is 0.9%. The latter is dominated by the luminosity measurement, which is needed for the normalization of the data set. We consider the good agreement between the $\mu^+\mu^-\gamma$ QED prediction and data as a validation of the accuracy of our efficiency corrections. As a further cross check, we have applied the efficiency corrections also to a statistically independent $\mu^+\mu^-\gamma$ sample, resulting in a difference between data and MC of $(0.7 \pm 0.2)\%$ over the full mass range, where the error is statistical only.

6. Extraction of $\sigma(e^+e^- \to \pi^+\pi^-)$ and $|F_\pi^2|$

6.1. Methods

We finally extract $\sigma_{\pi\pi} = \sigma(e^+e^- \to \pi^+\pi^-)$ according to two independent normalization schemes. In the first method, we obtain the bare cross section, *i.e.*, the cross section corrected for vacuum polarization effects, according to the following formula:

$$\sigma^{\rm bare}_{\pi\pi(\gamma_{\rm FSR})} = \frac{N_{\pi\pi\gamma} \cdot (1 + \delta^{\pi\pi}_{\rm FSR})}{\mathcal{L} \cdot \epsilon^{\pi\pi\gamma}_{\rm global} \cdot H(s) \cdot \delta_{\rm vac}}\,, \tag{1}$$

where $N_{\pi\pi\gamma}$ is the number of signal events found in data after applying all selection requirements described above and an unfolding procedure to correct for the mass resolution, $\mathcal{L}$ the luminosity of the data set, and H the radiator function. The global efficiency $\epsilon^{\pi\pi\gamma}_{\rm global}$ is determined based on the signal MC by dividing the measured number of events after all selection requirements $N^{\rm true}_{\rm measured}$ by that of all generated events $N^{\rm true}_{\rm generated}$. The true MC sample is used, with the full θ_γ range, applying the efficiency corrections mentioned in Section 3.3 but without taking into account the detector resolution in the invariant mass m:

$$\epsilon_{\rm global}(m) = \frac{N^{\rm true}_{\rm measured}(m)}{N^{\rm true}_{\rm generated}(m)}\,. \tag{2}$$

The efficiency is found to depend slightly on $m_{\pi\pi}$ and ranges from 2.8% to 3.0% from lowest to highest $m_{\pi\pi}$. An unfolding procedure, which eliminates the effect of the detector resolution, is described

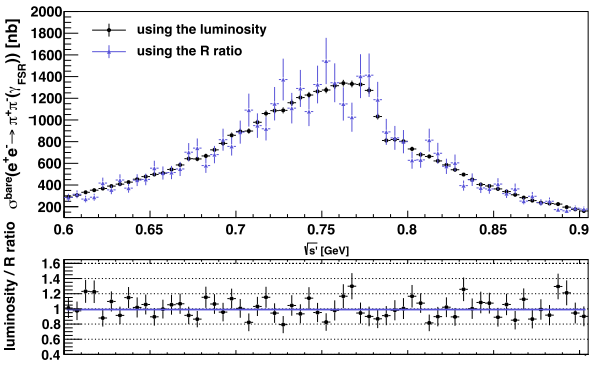

Fig. 2. Comparison between the methods to extract $\sigma_{\pi\pi}$ explained in the text — using the luminosity (black) and normalizing by $\sigma_{\mu\mu}$ (blue). The lower panel shows the ratio of these results together with a linear fit (blue line) to quantify their difference. (For interpretation of the references to color in this figure legend, the reader is referred to the web version of this article.)

in Sect. 6.2 and is applied before dividing by the global efficiency. The radiator function H is described in Sect. 6.4. As input for a_μ the bare cross section is needed. It can be obtained by dividing the cross section by the vacuum polarization correction $\delta_{\rm vac}$, which is also described in Sect. 6.4. As pointed out in Ref. [11], in order to consider radiative effects in the dispersion integral for a_μ, an FSR correction has to be performed. The determination of the correction factor $(1+\delta^{\pi\pi}_{\rm FSR})$ is described in Sect. 6.3.

In the second method, we use a different normalization than in the first method and normalize $N_{\pi\pi\gamma}$ to the measured number of $\mu^+\mu^-\gamma$ events, $N_{\mu\mu\gamma}$. Since $\mathcal{L}$, H, and $\delta_{\rm vac}$ cancel in this normalization, one finds the following formula:

$$\sigma^{\rm bare}_{\pi\pi(\gamma_{\rm FSR})} = \frac{N_{\pi\pi\gamma}}{N_{\mu\mu\gamma}} \cdot \frac{\epsilon^{\mu\mu\gamma}_{\rm global}}{\epsilon^{\pi\pi\gamma}_{\rm global}} \cdot \frac{1+\delta^{\mu\mu}_{\rm FSR}}{1+\delta^{\pi\pi}_{\rm FSR}} \cdot \sigma^{\rm bare}_{\mu\mu}\,, \tag{3}$$

where $\epsilon^{\mu\mu\gamma}_{\rm global}$ is the global efficiency of the dimuon selection, already described in Sect. 5, $\delta^{\mu\mu}_{\rm FSR}$ is the FSR correction factor to the $\mu^+\mu^-$ final state, which can be obtained using the Phokhara event generator, $\sigma^{\rm bare}_{\mu\mu}$ is the exact QED prediction of the dimuon cross section, given by [26, Eq. (5.13)]

$$\sigma^{\rm bare}_{\mu\mu} = \frac{4\pi\alpha^2}{3s'} \cdot \frac{\beta_\mu(3-\beta_\mu^2)}{2}\,, \tag{4}$$

with the fine structure constant α, the cms energy $s' < s$ available for the creation of the final state, the muon velocity $\beta_\mu = \sqrt{1-4m_\mu^2/s'}$, and the muon mass m_μ. The contributions of radiator function, luminosity, and vacuum polarization to the systematic uncertainties of the bare cross section, cancel in the second method. The upper panel of Fig. 2 shows the comparison of the bare cross sections including FSR obtained with the first (black) and second method before unfolding (blue). The error bars are statistical only. They are much larger for the second method due to the limited $\mu^+\mu^-\gamma$ statistics in the mass range of interest. The lower panel shows the ratio of these cross sections. Again, a linear fit is performed to quantify the difference, which is found to be $(0.85\pm1.68)\%$ and $\chi^2/{\rm ndf} = 50/60$, where the error is statistical. Both methods agree within uncertainties. The first one is used in the analysis. Finally, the pion form factor as a function of s' can be calculated via

$$|F_\pi|^2(s') = \frac{3s'}{\pi\alpha^2\beta_\pi^3(s')}\sigma^{\rm dressed}_{\pi\pi}(s')\,, \tag{5}$$

with the pion velocity $\beta_\pi(s') = \sqrt{1-4m_\pi^2/s'}$, the charged pion mass m_π, and the dressed cross section $\sigma^{\rm dressed}_{\pi\pi}(s') = \sigma(e^+e^-\to\pi^+\pi^-)(s')$ containing vacuum polarization, but corrected for FSR effects. The result is presented in Sect. 7.

6.2. Unfolding

In order to obtain the final result for $\sigma_{\pi\pi}$, one has to rectify the detector resolution effects, *i.e.*, the mass spectrum needs to be unfolded. To this end, the Singular Value Decomposition (SVD) method [27] is used. It requires two input variables — the response matrix and the regularization parameter τ. The SVD algorithm calculates an operator which cancels the detector smearing by inverting the response matrix. We obtain the response matrix in the full mass range between threshold and 3.0 GeV, using a signal MC sample. The matrix corresponds to the correlation of the reconstructed $m_{\pi\pi}$ spectrum, and the originally generated $m_{\pi\pi}$ values. With the choice of a bin width of 5 MeV/c^2, about 43% of events are found to be on the diagonal axis.

To find the value of the regularization parameter τ, we compare two independent methods, as suggested in Ref. [27]. On the one hand, we perform a MC simulation where τ is optimized such that unfolded and true distributions have the best agreement. On the other hand, we process an algorithm, described in [27], exploiting the singular values of the response matrix. Both methods favor a similar regularization parameter of $\tau \cong 72$.

To estimate the systematic uncertainties and to test the stability of the SVD method, we perform two cross checks. In both cases we use a $\pi^+\pi^-\gamma$ MC sample which is independent of the one used to determine the response matrix. We modify and then unfold the spectra in both checks. In the first cross check, the reconstructed spectrum is smeared with an additional Gaussian error, which results in an about 20% larger detector smearing than expected from MC simulation. The resulting unfolded spectrum reproduces the true one on the sub- per mille level. In the second cross check, the mass of the ρ-resonance is varied systematically in the simulation in steps of 10 MeV/c^2 between 750 and 790 MeV/c^2. The response matrix is kept fixed and was determined with a ρ mass of 770 MeV/c^2. In all cases, the masses of the ρ peak after unfolding are found to be close to the initially simulated masses. From the comparisons of these checks, we take the maximum deviation of 0.2% as systematic uncertainty.

6.3. FSR correction

The correction factor $\delta_{\rm FSR}$ is determined with the Phokhara generator in bins of $m_{\pi\pi}$. Two different correction methods are used on the data to cross check whether it is applied correctly.

(1) The whole FSR contribution of the $\pi^+\pi^-\gamma$ events is calculated with Phokhara, by dividing a true MC spectrum including FSR in NLO by the spectrum without any FSR contribution. The resulting distribution is used to correct data. As pointed out in Ref. [11], for the dispersion integral for a_μ, the FSR correction for the process $e^+e^-\to\pi^+\pi^-$ needs then to be added again. We use the calculation by Schwinger assuming point-like pions:

$$\sigma^{\rm dressed}_{\pi\pi(\gamma)} = \sigma^{\rm dressed}_{\pi\pi} \cdot \left[1+\eta(s)\frac{\alpha}{\pi}\right], \tag{6}$$

where $\eta(s)$ is the theoretical correction factor taken from [28]. In the ρ-peak region it is between 0.4% and 0.9%.

(2) A special version of the Phokhara generator is used [29], which, in contrast to the standard version of the generator, distinguishes whether a photon is emitted in the initial or the final state. In events in which photons have been radiated solely due to ISR, the momentum transfer of the virtual photon s_{γ^*} is equal to the invariant mass of the two pions $m^2_{\pi\pi}$. However, if an FSR

photon is emitted, the invariant mass is lowered due to this effect and hence $m^2_{\pi\pi} < s_{\gamma^*}$. The effect can be removed by applying an unfolding procedure, using again the SVD algorithm. Here, the response matrix is $m^2_{\pi\pi}$ vs. s_{γ^*}, obtained from a MC sample that includes FSR in NLO. The regularization parameter τ is determined as described in Sect. 6.2. After applying the corrections for the radiative $\pi^+\pi^-\gamma$ process, which are of the order of 2%, one obtains the $\pi^+\pi^-(\gamma_{\rm FSR})$ cross section directly.

The difference between both methods is found to be (0.18 ± 0.13)%. Both methods are complementary and agree with each other within errors. The difference is taken as systematic uncertainty. Finally, the correction obtained with method (1) is used in the analysis.

6.4. Radiator function and vacuum polarization correction

The radiator function is implemented within the Phokhara event generator with NLO precision. Hence, a very precise description is available with a claimed uncertainty of 0.5% [16].

To obtain the *bare* cross section, vacuum polarization effects $\delta_{\rm vac}$ must be taken into account. To this aim, the dressed cross section, including the vacuum polarization effects, is adjusted for the running of the coupling constant α [30]. Bare and dressed cross sections are related as follows:

$$\sigma^{\rm bare} = \frac{\sigma^{\rm dressed}}{\delta_{\rm vac}} = \sigma^{\rm dressed} \cdot \left(\frac{\alpha(0)}{\alpha(s)}\right)^2 . \quad (7)$$

The correction factors are taken from Ref. [31].

6.5. Summary of systematic uncertainties

Systematic uncertainties are studied within the investigated $m_{\pi\pi}$ range between 600 and 900 MeV/c^2. Sources are:

(1) Efficiency corrections: Each individual uncertainty is studied in bins of $m_{\pi\pi}$ with respect to three different sources. Firstly, the remaining background contaminations in the data samples are estimated with the corresponding MC simulation mentioned in Table 1. Their contribution is taken into account by multiplying the claimed uncertainties of the event generators and their fraction of the investigated signal events. Secondly, we vary the selection requirements (E/p, χ^2_{1C}, depth of a charged track in the MUC), which are used to select clean muon and pion samples for the efficiency studies, in a range of three times the resolution of the corresponding variable. The differences of the correction factors are calculated. Thirdly, the resolution of the correction factors, *i.e.*, the bin sizes of momentum and θ distributions, is varied by a factor two and the effects on the final correction factors are tested.

(2) Pion–muon separation: Additional uncertainties of using the ANN method for pion–muon separation are estimated by comparing the result from a different multivariate method, namely the Boosted Decision Tree (BDT) approach [23]. As a further cross check, the whole analysis is repeated without the use of a dedicated PID method.

(3) Residual background is subtracted using simulated events. The uncertainty is determined to be 0.1%.

(4) Angular acceptance: The knowledge of the angular acceptance of the tracks is studied by varying this requirement by more than three standard deviations of the angular resolution and studying the corresponding difference in the selected number of events. A difference of 0.1% in the result can be observed. The procedure is repeated for all other selection criteria. Their contribution to the total systematic uncertainty is found to be negligible.

(5) Unfolding: Uncertainties introduced by unfolding are smaller than 0.2%, as estimated by the two cross checks mentioned in Sect. 6.2.

Table 2
Summary of systematic uncertainties.

Source	Uncertainty (%)
Photon efficiency correction	0.2
Pion tracking efficiency correction	0.3
Pion ANN efficiency correction	0.2
Pion e-PID efficiency correction	0.2
ANN	negl.
Angular acceptance	0.1
Background subtraction	0.1
Unfolding	0.2
FSR correction $\delta_{\rm FSR}$	0.2
Vacuum polarization correction $\delta_{\rm vac}$	0.2
Radiator function	0.5
Luminosity $\mathcal{L}$	0.5
Sum	0.9

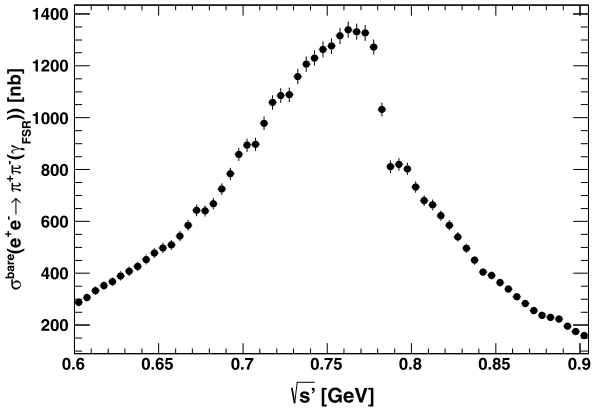

Fig. 3. The measured bare $e^+e^- \to \pi^+\pi^-(\gamma_{\rm FSR})$ cross section. Only the statistical errors are shown.

(6) FSR correction: The uncertainty due to the FSR correction is obtained by comparing two different approaches as described in Sect. 6.3. The uncertainty is found to be 0.2%.

(7) Vacuum Polarization: The uncertainty due to the vacuum polarization correction is conservatively estimated to be 0.2%.

(8) Radiator Function: The Radiator Function extracted from the Phokhara generator is implemented with a precision of 0.5%.

(9) Luminosity: The luminosity of the analyzed data set has been determined to a precision of 0.5%.

All systematic uncertainties are summarized in Table 2. They are added in quadrature, and a total systematic uncertainty for $\sigma^{\rm bare}(e^+e^- \to \pi^+\pi^-(\gamma_{\rm FSR}))$ of 0.9% is achieved, which is fully correlated amongst all data points.

7. Results

The result for $\sigma^{\rm bare}(e^+e^- \to \pi^+\pi^-(\gamma_{\rm FSR}))$ as a function of $\sqrt{s} = m_{\pi\pi}$ is illustrated in Fig. 3 and given numerically in Table 4. The cross section is corrected for vacuum polarization effects and includes final state radiation. Besides the dominant $\rho(770)$ peak, the well-known structure of the ρ–ω interference is observed. The result for the pion form factor $|F_\pi|^2$ is shown in Fig. 4 and given numerically in Table 4. It includes vacuum polarization corrections, but, differently from the cross section shown in Fig. 3, final state radiation effects are excluded here. The red line in Fig. 4 illustrates a fit to data according to a parametrization proposed by Gounaris and Sakurai [32]. Here, exactly the same fit formula and fit procedure are applied as described in detail in Ref. [10]. Free parameters of the fit are the mass and width Γ of the ρ meson, the mass of the ω meson, and the phase of the Breit–

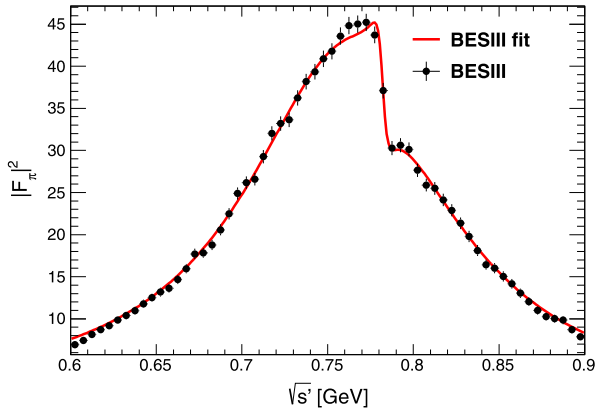

Fig. 4. The measured squared pion form factor $|F_\pi|^2$. Only statistical errors are shown. The solid line represents the fit using the Gounaris–Sakurai parametrization.

Table 3
Fit parameters and statistical errors of the Gounaris–Sakurai fit of the pion form factor. Also shown are the PDG 2014 values [33].

Parameter	BESIII value	PDG 2014
m_ρ [MeV/c^2]	776.0 ± 0.4	775.26 ± 0.25
Γ_ρ [MeV]	151.7 ± 0.7	147.8± 0.9
m_ω [MeV/c^2]	782.2 ± 0.6	782.65 ± 0.12
Γ_ω [MeV]	fixed to PDG	8.49 ± 0.08
$\lvert c_\omega\rvert$ [10^{-3}]	1.7± 0.2	–
$\lvert\phi_\omega\rvert$ [rad]	0.04 ± 0.13	–

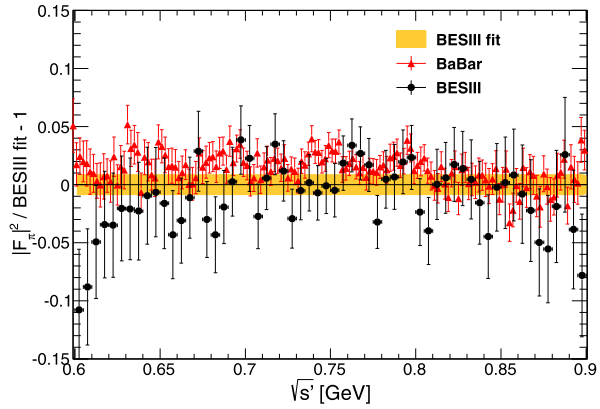

Fig. 5. Relative difference of the form factor squared from BaBar [10] and the BESIII fit. Statistical and systematic uncertainties are included in the data points. The width of the BESIII band shows the systematic uncertainty only.

Wigner function $c_\omega = |c_\omega| e^{i\phi_\omega}$. The width of the ω meson is fixed to the PDG value [33]. The resulting values are shown in Table 3. As can be seen, the resonance parameters are in agreement with the PDG values [33] within uncertainties, except for Γ_ρ, which shows a 3.4σ deviation. Corresponding amplitudes for the higher ρ states, $\rho(1450)$, $\rho(1700)$, and $\rho(2150)$, as well as the masses and widths of those states were taken from Ref. [10], and the systematic uncertainty in Γ_ρ due to these assumptions has not been quantitatively evaluated.

The Gounaris–Sakurai fit provides an excellent description of the BESIII data in the full mass range from 600 to 900 MeV/c^2, resulting in $\chi^2/\text{ndf} = 49.1/56$. Fig. 5 shows the difference between fit and data. Here the data points show the statistical uncertainties only, while the shaded error band of the fit shows the systematic uncertainty only.

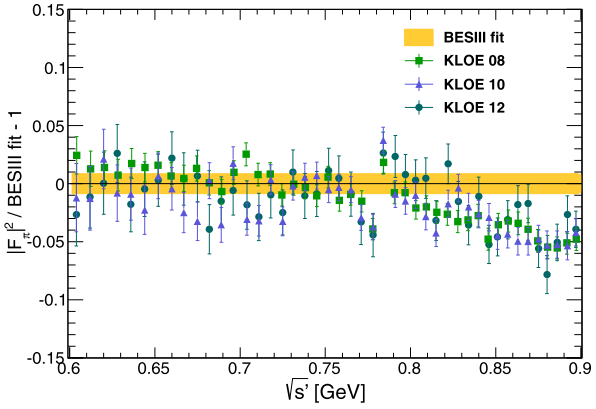

Fig. 6. Relative difference of the form factor squared from KLOE [6–8] and the BESIII fit. Statistical and systematic uncertainties are included in the data points. The width of the BESIII band shows the systematic uncertainty only.

In order to compare the result with previous measurements, the relative difference of the BESIII fit and data from BaBar [10], KLOE [6–8], CMD2 [1,2], and SND [3] is investigated. Such a comparison is complicated by the fact, that previous measurements used different vacuum polarization corrections. Therefore, we consistently used the vacuum polarization correction from Ref. [31] for all the comparisons discussed in this section. The KLOE 08, 10, 12, and BaBar spectra have, hence, been modified accordingly. The individual comparisons are illustrated in Figs. 5 and 6. Here, the shaded error band of the fit includes the systematic error only, while the uncertainties of the data points include the sum of the statistical and systematic errors. We observe a very good agreement with the KLOE 08 and KLOE 12 data sets up to the mass range of the ρ–ω interference. In the same mass range the BaBar and KLOE 10 data sets show a systematic shift, however, the deviation is, not exceeding 1 to 2 standard deviations. At higher masses, the statistical error bars in the case of BESIII are relatively large, such that a comparison is not conclusive. There seem to be a good agreement with the BaBar data, while a large deviation with all three KLOE data sets is visible. There are indications that the BESIII data and BESIII fit show some disagreement in the low mass and very high mass tails as well. We have also compared our results in the ρ peak region with data from Novosibirsk. At lower and higher masses, the statistical uncertainties of the Novosibirsk results are too large to draw definite conclusions. The spectra from SND and from the 2006 publication of CMD-2 are found to be in very good agreement with BESIII in the ρ peak region, while the 2004 result of CMD-2 shows a systematic deviation of a few percent.

We also compute the contribution of our BESIII cross section measurement $\sigma^{\text{bare}}(e^+e^- \to \pi^+\pi^-(\gamma_{\text{FSR}}))$ to the hadronic contribution of $(g-2)_\mu$,

$$a_\mu^{\pi\pi,\text{LO}}(0.6\text{–}0.9\,\text{GeV}) = \frac{1}{4\pi^3}\int_{(0.6\text{GeV})^2}^{(0.9\text{GeV})^2} ds' K(s')\sigma^{\text{bare}}_{\pi\pi(\gamma)}\,, \tag{8}$$

where $K(s')$ is the kernel function [11, Eq. (5)]. As summarized in Fig. 7, the BESIII result, $a_\mu^{\pi\pi,\text{LO}}(600\text{–}900\ \text{MeV}) = (368.2 \pm 2.5_{\text{stat}} \pm 3.3_{\text{sys}}) \cdot 10^{-10}$, is found to be in good agreement with all three KLOE values. A difference of about 1.7σ with respect to the BaBar result is observed.

Table 4
Results of the BESIII measurement of the cross section $\sigma^{\rm bare}_{\pi^+\pi^-(\gamma_{\rm FSR})} \equiv \sigma^{\rm bare}(e^+e^- \to \pi^+\pi^-(\gamma_{\rm FSR}))$ and the squared pion form factor $|F_\pi|^2$. The errors are statistical only. The value of $\sqrt{s'}$ represents the bin center. The 0.9% systematic uncertainty is fully correlated between any two bins.

$\sqrt{s'}$ [MeV]	$\sigma^{\rm bare}_{\pi^+\pi^-(\gamma_{\rm FSR})}$ [nb]	$\lvert F_\pi\rvert^2$	$\sqrt{s'}$ [MeV]	$\sigma^{\rm bare}_{\pi^+\pi^-(\gamma_{\rm FSR})}$ [nb]	$\lvert F_\pi\rvert^2$
602.5	288.3 ± 15.2	6.9 ± 0.4	752.5	1276.1 ± 29.8	41.8 ± 1.0
607.5	306.6 ± 15.5	7.4 ± 0.4	757.5	1315.9 ± 31.3	43.6 ± 1.0
612.5	332.8 ± 16.3	8.2 ± 0.4	762.5	1339.3 ± 30.9	44.8 ± 1.0
617.5	352.5 ± 16.3	8.7 ± 0.4	767.5	1331.9 ± 30.8	45.0 ± 1.0
622.5	367.7 ± 16.6	9.2 ± 0.4	772.5	1327.0 ± 30.6	45.2 ± 1.0
627.5	390.1 ± 17.7	9.8 ± 0.4	777.5	1272.7 ± 29.2	43.7 ± 1.0
632.5	408.0 ± 18.0	10.4 ± 0.5	782.5	1031.5 ± 26.7	37.1 ± 0.9
637.5	426.6 ± 18.1	11.0 ± 0.5	787.5	810.7 ± 24.2	30.3 ± 0.8
642.5	453.5 ± 19.0	11.8 ± 0.5	792.5	819.7 ± 23.8	30.6 ± 0.8
647.5	477.7 ± 18.5	12.5 ± 0.5	797.5	803.1 ± 23.3	30.1 ± 0.8
652.5	497.4 ± 19.5	13.2 ± 0.5	802.5	732.4 ± 22.1	27.7 ± 0.8
657.5	509.2 ± 19.4	13.6 ± 0.5	807.5	679.9 ± 20.6	25.9 ± 0.7
662.5	543.4 ± 19.9	14.7 ± 0.5	812.5	663.6 ± 21.0	25.5 ± 0.8
667.5	585.0 ± 20.5	16.0 ± 0.6	817.5	622.2 ± 19.9	24.1 ± 0.7
672.5	642.7 ± 22.2	17.7 ± 0.6	822.5	585.0 ± 19.5	22.9 ± 0.7
677.5	640.5 ± 21.0	17.8 ± 0.6	827.5	540.8 ± 18.1	21.4 ± 0.7
682.5	668.0 ± 21.9	18.8 ± 0.6	832.5	496.4 ± 17.7	19.8 ± 0.7
687.5	724.4 ± 22.9	20.6 ± 0.6	837.5	450.4 ± 16.8	18.1 ± 0.6
692.5	783.5 ± 23.2	22.5 ± 0.7	842.5	404.7 ± 15.2	16.4 ± 0.6
697.5	858.6 ± 25.3	24.9 ± 0.7	847.5	391.3 ± 15.4	16.0 ± 0.6
702.5	893.8 ± 25.4	26.2 ± 0.7	852.5	364.0 ± 15.0	15.0 ± 0.6
707.5	897.8 ± 25.0	26.6 ± 0.7	857.5	339.6 ± 14.0	14.2 ± 0.6
712.5	978.6 ± 26.6	29.3 ± 0.8	862.5	310.0 ± 13.7	13.0 ± 0.6
717.5	1059.1 ± 27.9	32.0 ± 0.8	867.5	283.8 ± 13.0	12.1 ± 0.5
722.5	1086.0 ± 28.3	33.2 ± 0.9	872.5	256.5 ± 12.4	11.0 ± 0.5
727.5	1088.4 ± 27.7	33.6 ± 0.9	877.5	237.3 ± 11.4	10.3 ± 0.5
732.5	1158.8 ± 29.2	36.2 ± 0.9	882.5	229.7 ± 11.6	10.0 ± 0.5
737.5	1206.5 ± 29.6	38.2 ± 0.9	887.5	224.0 ± 11.6	9.9 ± 0.5
742.5	1229.9 ± 29.0	39.3 ± 0.9	892.5	196.1 ± 10.5	8.7 ± 0.4
747.5	1263.3 ± 30.3	40.9 ± 1.0	897.5	175.9 ± 9.7	7.9 ± 0.4

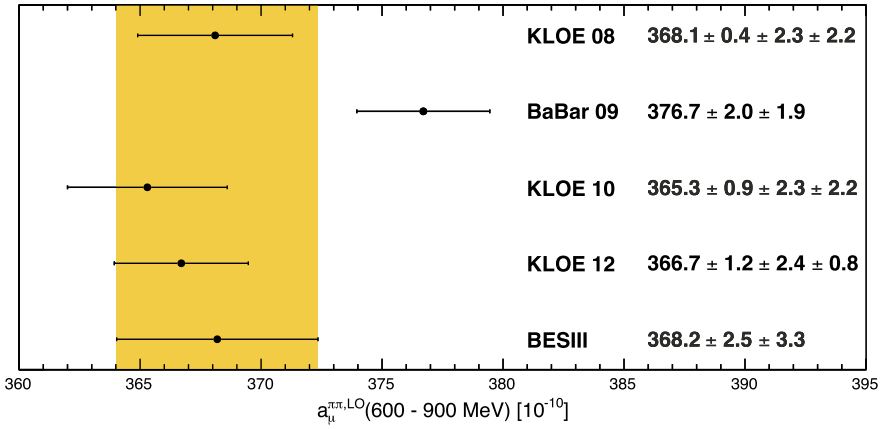

Fig. 7. Our calculation of the leading-order (LO) hadronic vacuum polarization 2π contributions to $(g-2)_\mu$ in the energy range 600–900 MeV from BESIII and based on the data from KLOE 08 [6], 10 [7], 12 [8], and BaBar [10], with the statistical and systematic errors. The statistical and systematic errors are added quadratically. The band shows the 1σ range of the BESIII result.

8. Conclusion

A new measurement of the cross section $\sigma^{\rm bare}(e^+e^- \to \pi^+\pi^-(\gamma_{\rm FSR}))$ has been performed with an accuracy of 0.9% in the dominant $\rho(770)$ mass region between 600 and 900 MeV/c^2, using the ISR method at BESIII. The energy dependence of the cross section appears compatible with corresponding measurements from KLOE and BaBar within approximately one standard deviation. The two-pion contribution to the hadronic vacuum polarization contribution to $(g-2)_\mu$ has been determined from the BESIII data to be $a_\mu^{\pi\pi,\rm LO}(600\text{–}900\ \text{MeV}) = (368.2 \pm 2.5_{\rm stat} \pm 3.3_{\rm sys}) \cdot 10^{-10}$. By averaging the KLOE, BaBar, and BESIII values of $a_\mu^{\pi\pi,\rm LO}$ and assuming that the five data sets are independent, a deviation of more than 3σ between the SM prediction of $(g-2)_\mu$ and its direct measurement is confirmed. For the low mass region < 600 MeV/c^2 and the high mass region > 900 MeV/c^2, the BaBar data was used in this calculation.

Acknowledgements

The BESIII Collaboration thanks the staff of BEPCII and the IHEP computing center for their strong support. We thank Thomas Teubner for the recalculation of $a_\mu^{\pi\pi,\rm LO}$(600–900 MeV) and Fedor Ignatov for the useful discussions. This work is supported in part by National Key Basic Research Program of China under Contract No. 2015CB856700; National Natural Science Foundation of China (NSFC) under Contract Nos. 11125525, 11235011, 11322544, 11335008, 11425524; the Chinese Academy of Sciences (CAS) Large-Scale Scientific Facility Program; the CAS Center for Excel-

lence in Particle Physics (CCEPP); the Collaborative Innovation Center for Particles and Interactions (CICPI); Joint Large-Scale Scientific Facility Funds of the NSFC and CAS under Contract Nos. 11179007, U1232201, U1332201; CAS under Contract Nos. KJCX2-YW-N29, KJCX2-YW-N45; 100 Talents Program of CAS; National 1000 Talents Program of China; INPAC and Shanghai Key Laboratory for Particle Physics and Cosmology; German Research Foundation DFG under Contract No. Collaborative Research Center CRC-1044; Istituto Nazionale di Fisica Nucleare, Italy; Ministry of Development of Turkey under Contract No. DPT2006K-120470; Russian Foundation for Basic Research under Contract No. 14-07-91152; The Swedish Resarch Council; U.S. Department of Energy under Contract Nos. DE-FG02-04ER41291, DE-FG02-05ER41374, DE-FG02-94ER40823, DESC0010118; U.S. National Science Foundation; University of Groningen (RuG) and the Helmholtzzentrum für Schwerionenforschung GmbH (GSI), Darmstadt; WCU Program of National Research Foundation of Korea under Contract No. R32-2008-000-10155-0.

Appendix A. Supplementary material

Supplementary material related to this article can be found online at http://dx.doi.org/10.1016/j.physletb.2015.11.043.

References

[1] R.R. Akhmetshin, et al., CMD2 Collaboration, Phys. Lett. B 578 (2004) 285.
[2] R.R. Akhmetshin, et al., CMD2 Collaboration, Phys. Lett. B 648 (2007) 28.
[3] M.N. Achasov, et al., SND Collaboration, J. Exp. Theor. Phys. 101 (2005) 1053.
[4] J.E. Augustin, et al., Phys. Rev. Lett. 20 (1968) 126.
[5] A. Aloisio, et al., KLOE Collaboration, Phys. Lett. B 606 (2005) 12.
[6] F. Ambrosio, et al., KLOE Collaboration, Phys. Lett. B 670 (2009) 285.
[7] F. Ambrosino, et al., KLOE Collaboration, Phys. Lett. B 700 (2011) 102.
[8] D. Babusci, et al., KLOE Collaboration, Phys. Lett. B 720 (2013) 336.
[9] B. Aubert, et al., BABAR Collaboration, Phys. Rev. Lett. 103 (2009) 231801.
[10] J.P. Lees, et al., BABAR Collaboration, Phys. Rev. D 86 (2012) 032013.
[11] S. Eidelman, F. Jegerlehner, Z. Phys. C 67 (1995) 585.
[12] M. Davier, A. Hoecker, B. Malescu, Z. Zhang, Eur. Phys. J. C 71 (2011) 1515.
[13] K. Hagiwara, R. Liao, A.D. Martin, Daisuke Nomura, T. Teubner, J. Phys. G 38 (2011) 085003.
[14] M. Davier, A. Hoecker, B. Malescu, C.Z. Yuan, Z. Zhang, Eur. Phys. J. C 66 (2010) 1.
[15] M. Ablikim, et al., BESIII Collaboration, Nucl. Instrum. Methods, Sect. A 614 (2010) 345.
[16] G. Rodrigo, H. Czyż, J.H. Kuhn, M. Szopa, Eur. Phys. J. C 24 (2002) 71.
[17] H. Czyż, J.H. Kuhn, A. Wapienik, Phys. Rev. D 77 (2008) 114005.
[18] S. Jadach, B.F.L. Ward, Z. Was, Comput. Phys. Commun. 130 (2000) 260.
[19] G. Balossini, C.M.C. Calame, G. Montagna, O. Nicrosini, F. Piccinini, Nucl. Phys. B 758 (2006) 227.
[20] J. Allison, et al., GEANT4 Collaboration, IEEE Trans. Nucl. Sci. 53 (2006) 270.
[21] S. Agostinelli, et al., GEANT4 Collaboration, Nucl. Instrum. Methods, Sect. A 506 (2003) 250.
[22] D.M. Asner, et al., Int. J. Mod. Phys. A 24 (2009) 1.
[23] A. Hoecker, P. Speckmayer, J. Stelzer, J. Therhaag, E. Von Toerne, H. Voss, PoS ACAT 040 (2007).
[24] M. Ablikim, et al., BESIII Collaboration, Chin. Phys. C 37 (2013) 123001.
[25] G. Balossini, C. Bignamini, C.M. Carloni Calame, G. Montagna, F. Piccinini, O. Nicrosini, Phys. Lett. B 663 (2008) 209.
[26] M.E. Peskin, D.V. Schroeder, An Introduction to Quantum Field Theory, vol. 2, Addison–Wesley, USA, 1995, p. 135.
[27] A. Hoecker, V. Kartvelishvili, Nucl. Instrum. Methods, Sect. A 372 (1996) 469.
[28] J.S. Schwinger, Particles, Sources and Fields, vol. 3, Addison–Wesley, Redwood City, USA, 1989, p. 99 ff.
[29] Private communication with H. Czyz.
[30] A. Höfer, J. Gluza, F. Jegerlehner, Eur. Phys. J. C 24 (2002) 51.
[31] F. Jegerlehner, Nucl. Phys. Proc. Suppl. 181–182 (2008) 135;
F. Jegerlehner, Z. Phys. C 32 (1986) 195;
F. Jegerlehner, www-com.physik.hu-berlin.de/~fjeger/alphaQED.tar.gz, 2015.
[32] G.J. Gounaris, J.J. Sakurai, Phys. Rev. Lett. 21 (1968) 244.
[33] K.A. Olive, et al., Particle Data Group, Chin. Phys. C 38 (2014) 090001.

Update

Physics Letters B

Volume 812, Issue , 10 January 2021, Page

DOI: https://doi.org/10.1016/j.physletb.2020.135982

Physics Letters B 812 (2021) 135982

Contents lists available at ScienceDirect

Physics Letters B

www.elsevier.com/locate/physletb

Corrigendum

Corrigendum to "Measurement of the $e^+e^- \to \pi^+\pi^-$ cross section between 600 and 900 MeV using initial state radiation" [Phys. Lett. B 753 (2016) 629–638]

BESIII Collaboration

M. Ablikim [a], M.N. Achasov [j,3], P. Adlarson [bv], S. Ahmed [o], M. Albrecht [d], R. Aliberti [ad], A. Amoroso [bu,z], Q. An [br,ay,az], X.H. Bai [bk], Y. Bai [ax], O. Bakina [ae], R. Baldini Ferroli [w], I. Balossino [x], Y. Ban [an,11], K. Begzsuren [ab], N. Berger [ad], M. Bertani [w], D. Bettoni [x], F. Bianchi [bu,z], J. Biernat [bv], J. Bloms [bn], A. Bortone [bu,z], I. Boyko [ae], R.A. Briere [e], H. Cai [bw], X. Cai [a,ay,az], A. Calcaterra [w], G.F. Cao [a,bf], N. Cao [a,bf], S.A. Cetin [be], J.F. Chang [a,ay,az], W.L. Chang [a,bf], G. Chelkov [ae,2], D.Y. Chen [f], G. Chen [a], H.S. Chen [a,bf], M.L. Chen [a,ay,az], S.J. Chen [ak], X.R. Chen [aa], Y.B. Chen [a,ay,az], Z.J. Chen [t,12], W.S. Cheng [z], G. Cibinetto [x], F. Cossio [z], X.F. Cui [al], H.L. Dai [a,ay,az], X.C. Dai [a,bf], A. Dbeyssi [o], R.E. de Boer [d], D. Dedovich [ae], Z.Y. Deng [a], A. Denig [ad], I. Denysenko [ae], M. Destefanis [bu,z], F. De Mori [bu,z], Y. Ding [ai], C. Dong [al], J. Dong [a,ay,az], L.Y. Dong [a,bf], M.Y. Dong [a,ay,az,bf], X. Dong [bw], S.X. Du [bz], J. Fang [a,ay,az], S.S. Fang [a,bf], Y. Fang [a], R. Farinelli [x], L. Fava [bg,z], F. Feldbauer [d], G. Felici [w], C.Q. Feng [br,ay,az], M. Fritsch [d], C.D. Fu [a], Y. Gao [bs], Y. Gao [br,ay,az], Y. Gao [an,11], Y.G. Gao [f], I. Garzia [x,bh], E.M. Gersabeck [bl], A. Gilman [bm], K. Goetzen [k], L. Gong [ai], W.X. Gong [a,ay,az], W. Gradl [ad], M. Greco [bu,z], L.M. Gu [ak], M.H. Gu [a,ay,az], S. Gu [b], Y.T. Gu [m], C.Y. Guan [a,bf], A.Q. Guo [v], L.B. Guo [aj], R.P. Guo [ap], Y.P. Guo [i,8], A. Guskov [ae], T.T. Han [aq], X.Q. Hao [p], F.A. Harris [bj], K.L. He [a,bf], F.H. Heinsius [d], C.H. Heinz [ad], T. Held [d], Y.K. Heng [a,ay,az,bf], C. Herold [bb], M. Himmelreich [k,6], T. Holtmann [d], Y.R. Hou [bf], Z.L. Hou [a], H.M. Hu [a,bf], J.F. Hu [aw,13], T. Hu [a,ay,az,bf], Y. Hu [a], G.S. Huang [br,ay,az], L.Q. Huang [bs], X.T. Huang [aq], Y.P. Huang [a], Z. Huang [an,11], N. Huesken [bn], T. Hussain [bt], W. Ikegami Andersson [bv], W. Imoehl [v], M. Irshad [br,ay,az], S. Jaeger [d], S. Janchiv [ab,10], Q. Ji [a], Q.P. Ji [p], X.B. Ji [a,bf], X.L. Ji [a,ay,az], H.B. Jiang [aq], X.S. Jiang [a,ay,az,bf], J.B. Jiao [aq], Z. Jiao [r], S. Jin [ak], Y. Jin [bk],

DOI of original article: https://doi.org/10.1016/j.physletb.2015.11.043.

E-mail address: redmer@uni-mainz.de (C.F. Redmer).

[1] Also at Bogazici University, 34342 Istanbul, Turkey.

[2] Also at the Moscow Institute of Physics and Technology, Moscow 141700, Russia.

[3] Also at the Novosibirsk State University, Novosibirsk, 630090, Russia.

[4] Also at the NRC "Kurchatov Institute", PNPI, 188300, Gatchina, Russia.

[5] Also at Istanbul Arel University, 34295 Istanbul, Turkey.

[6] Also at Goethe University Frankfurt, 60323 Frankfurt am Main, Germany.

[7] Also at Key Laboratory for Particle Physics, Astrophysics and Cosmology, Ministry of Education; Shanghai Key Laboratory for Particle Physics and Cosmology; Institute of Nuclear and Particle Physics, Shanghai 200240, People's Republic of China.

[8] Also at Key Laboratory of Nuclear Physics and Ion-beam Application (MOE) and Institute of Modern Physics, Fudan University, Shanghai 200443, People's Republic of China.

[9] Also at Harvard University, Department of Physics, Cambridge, MA, 02138, USA.

[10] Currently at: Institute of Physics and Technology, Peace Ave.54B, Ulaanbaatar 13330, Mongolia.

[11] Also at State Key Laboratory of Nuclear Physics and Technology, Peking University, Beijing 100871, People's Republic of China.

[12] School of Physics and Electronics, Hunan University, Changsha 410082, China.

[13] Also at Guangdong Provincial Key Laboratory of Nuclear Science, Institute of Quantum Matter, South China Normal University, Guangzhou 510006, China.

https://doi.org/10.1016/j.physletb.2020.135982

T. Johansson [bv], N. Kalantar-Nayestanaki [bi], X.S. Kang [ai], R. Kappert [bi], M. Kavatsyuk [bi], B.C. Ke [as,a], I.K. Keshk [d], A. Khoukaz [bn], P. Kiese [ad], R. Kiuchi [a], R. Kliemt [k], L. Koch [af], O.B. Kolcu [be,5], B. Kopf [d], M. Kuemmel [d], M. Kuessner [d], A. Kupsc [bv], M.G. Kurth [a,bf], W. Kühn [af], J.J. Lane [bl], J.S. Lange [af], P. Larin [o], A. Lavania [u], L. Lavezzi [bu,z], Z.H. Lei [br,ay,az], H. Leithoff [ad], M. Lellmann [ad], T. Lenz [ad], C. Li [ao], C.H. Li [ah], Cheng Li [br,ay,az], D.M. Li [bz], F. Li [a,ay,az], G. Li [a], H. Li [as], H. Li [br,ay,az], H.B. Li [a,bf], H.J. Li [i,8], J.L. Li [aq], J.Q. Li [d], Ke Li [a], L.K. Li [a], Lei Li [c], P.L. Li [br,ay,az], P.R. Li [ag], S.Y. Li [bc], W.D. Li [a,bf], W.G. Li [a], X.H. Li [br,ay,az], X.L. Li [aq], Z.Y. Li [ba], H. Liang [br,ay,az], H. Liang [a,bf], H. Liang [ac], Y.F. Liang [au], Y.T. Liang [aa], G.R. Liao [l], L.Z. Liao [a,bf], J. Libby [u], C.X. Lin [ba], B.J. Liu [a], C.X. Liu [a], D. Liu [br,ay,az], F.H. Liu [at], Fang Liu [a], Feng Liu [f], H.B. Liu [m], H.M. Liu [a,bf], Huanhuan Liu [a], Huihui Liu [q], J.B. Liu [br,ay,az], J.Y. Liu [a,bf], K. Liu [a], K.Y. Liu [ai], Ke Liu [f], L. Liu [br,ay,az], M.H. Liu [i,8], Q. Liu [bf], S.B. Liu [br,ay,az], Shuai Liu [av], T. Liu [a,bf], W.M. Liu [br,ay,az], X. Liu [ag], Y.B. Liu [al], Z.A. Liu [a,ay,az,bf], Z.Q. Liu [aq], X.C. Lou [a,ay,az,bf], F.X. Lu [p], H.J. Lu [r], J.D. Lu [a,bf], J.G. Lu [a,ay,az], X.L. Lu [a], Y. Lu [a], Y.P. Lu [a,ay,az], C.L. Luo [aj], M.X. Luo [by], P.W. Luo [ba], T. Luo [i,8], X.L. Luo [a,ay,az], S. Lusso [z], X.R. Lyu [bf], F.C. Ma [ai], H.L. Ma [a], L.L. Ma [aq], M.M. Ma [a,bf], Q.M. Ma [a], R.Q. Ma [a,bf], R.T. Ma [bf], X.X. Ma [a,bf], X.Y. Ma [a,ay,az], F.E. Maas [o], M. Maggiora [bu,z], S. Maldaner [d], S. Malde [bp], Q.A. Malik [bt], A. Mangoni [y], Y.J. Mao [an,11], Z.P. Mao [a], S. Marcello [bu,z], Z.X. Meng [bk], J.G. Messchendorp [bi], G. Mezzadri [x], T.J. Min [ak], R.E. Mitchell [v], X.H. Mo [a,ay,az,bf], Y.J. Mo [f], N.Yu. Muchnoi [j,3], H. Muramatsu [bm], S. Nakhoul [k,6], Y. Nefedov [ae], F. Nerling [k,6], I.B. Nikolaev [j,3], Z. Ning [a,ay,az], S. Nisar [h,9], S.L. Olsen [bf], Q. Ouyang [a,ay,az,bf], S. Pacetti [y,bo], X. Pan [i,8], Y. Pan [bl], A. Pathak [a], P. Patteri [w], M. Pelizaeus [d], H.P. Peng [br,ay,az], K. Peters [k,6], J. Pettersson [bv], J.L. Ping [aj], R.G. Ping [a,bf], A. Pitka [d], R. Poling [bm], V. Prasad [br,ay,az], H. Qi [br,ay,az], H.R. Qi [bc], K.H. Qi [aa], M. Qi [ak], T.Y. Qi [i], T.Y. Qi [b], S. Qian [a,ay,az], W.-B. Qian [bf], Z. Qian [ba], C.F. Qiao [bf], L.Q. Qin [l], X.S. Qin [d], Z.H. Qin [a,ay,az], J.F. Qiu [a], S.Q. Qu [al], K. Ravindran [u], C.F. Redmer [ad], A. Rivetti [z], V. Rodin [bi], M. Rolo [z], G. Rong [a,bf], Ch. Rosner [o], M. Rump [bn], H.S. Sang [br], A. Sarantsev [ae,4], Y. Schelhaas [ad], C. Schnier [d], K. Schoenning [bv], M. Scodeggio [x,bh], D.C. Shan [av], W. Shan [s], X.Y. Shan [br,ay,az], M. Shao [br,ay,az], C.P. Shen [i], P.X. Shen [al], X.Y. Shen [a,bf], H.C. Shi [br,ay,az], R.S. Shi [a,bf], X. Shi [a,ay,az], X.D. Shi [br,ay,az], J.J. Song [aq], W.M. Song [ac,a], Y.X. Song [an,11], S. Sosio [bu,z], S. Spataro [bu,z], K.X. Su [bw], F.F. Sui [aq], G.X. Sun [a], H.K. Sun [a], J.F. Sun [p], L. Sun [bw], S.S. Sun [a,bf], T. Sun [a,bf], W.Y. Sun [aj], X. Sun [t,12], Y.J. Sun [br,ay,az], Y.K. Sun [br,ay,az], Y.Z. Sun [a], Z.T. Sun [a], Y.H. Tan [bw], Y.X. Tan [br,ay,az], C.J. Tang [au], G.Y. Tang [a], J. Tang [ba], J.X. Teng [br,ay,az], V. Thoren [bv], I. Uman [be], B. Wang [a], C.W. Wang [ak], D.Y. Wang [an,11], H.P. Wang [a,bf], K. Wang [a,ay,az], L.L. Wang [a], M. Wang [aq], M.Z. Wang [an,11], Meng Wang [a,bf], W.H. Wang [bw], W.P. Wang [br,ay,az], X. Wang [an,11], X.F. Wang [ag], X.L. Wang [i,8], Y. Wang [ba], Y. Wang [br,ay,az], Y.D. Wang [am], Y.F. Wang [a,ay,az,bf], Y.Q. Wang [a], Z. Wang [a,ay,az], Z.Y. Wang [a], Ziyi Wang [bf], Zongyuan Wang [a,bf], D.H. Wei [l], P. Weidenkaff [ad], F. Weidner [bn], S.P. Wen [a], D.J. White [bl], U. Wiedner [d], G. Wilkinson [bp], M. Wolke [bv], L. Wollenberg [d], J.F. Wu [a,bf], L.H. Wu [a], L.J. Wu [a,bf], X. Wu [i,8], Z. Wu [a,ay,az], L. Xia [br,ay,az], H. Xiao [i,8], S.Y. Xiao [a], Z.J. Xiao [aj], X.H. Xie [an,11], Y.G. Xie [a,ay,az], Y.H. Xie [f], T.Y. Xing [a,bf], G.F. Xu [a], J.J. Xu [ak], Q.J. Xu [n], W. Xu [a,bf], X.P. Xu [av], Y.C. Xu [bf], F. Yan [i,8], L. Yan [i,8], L. Yan [bu,z,8], W.B. Yan [br,ay,az], W.C. Yan [bz], Xu Yan [av], H.J. Yang [ar,7], H.X. Yang [a], L. Yang [as], S.L. Yang [bf], Y.H. Yang [ak], Y.X. Yang [l], Yifan Yang [a,bf], Zhi Yang [aa], M. Ye [a,ay,az], M.H. Ye [g], J.H. Yin [a], Z.Y. You [ba], B.X. Yu [a,ay,az,bf], C.X. Yu [al], G. Yu [a,bf], J.S. Yu [t,12], T. Yu [bs], C.Z. Yuan [a,bf], L. Yuan [b], W. Yuan [bu,z], X.Q. Yuan [an,11], Y. Yuan [a], Z.Y. Yuan [ba], C.X. Yue [ah], A. Yuncu [be,1], A.A. Zafar [bt], Y. Zeng [t,12], B.X. Zhang [a], Guangyi Zhang [p], H. Zhang [br], H.H. Zhang [ba], H.H. Zhang [ac], H.Y. Zhang [a,ay,az], J.J. Zhang [as], J.L. Zhang [bx], J.Q. Zhang [aj], J.W. Zhang [a,ay,az,bf], J.Y. Zhang [a], J.Z. Zhang [a,bf], Jianyu Zhang [a,bf], Jiawei Zhang [a,bf], Lei Zhang [ak], S. Zhang [ba], S.F. Zhang [ak], Shulei Zhang [t,12], X.D. Zhang [am], X.Y. Zhang [aq], Y. Zhang [bp], Y.H. Zhang [a,ay,az], Y.T. Zhang [br,ay,az], Yan Zhang [br,ay,az], Yao Zhang [a], Yi Zhang [i,8], Z.H. Zhang [f], Z.Y. Zhang [bw], G. Zhao [a], J. Zhao [ah], J.Y. Zhao [a,bf], J.Z. Zhao [a,ay,az], Lei Zhao [br,ay,az], Ling Zhao [a], M.G. Zhao [al], Q. Zhao [a], S.J. Zhao [bz], Y.B. Zhao [a,ay,az], Y.X. Zhao [aa], Z.G. Zhao [br,ay,az], A. Zhemchugov [ae,2], B. Zheng [bs], J.P. Zheng [a,ay,az], Y. Zheng [an,11], Y.H. Zheng [bf], B. Zhong [aj], C. Zhong [bs], L.P. Zhou [a,bf], Q. Zhou [a,bf], X. Zhou [bw], X.K. Zhou [bf], X.R. Zhou [br,ay,az], A.N. Zhu [a,bf], J. Zhu [al], K. Zhu [a],

K.J. Zhu [a,ay,az,bf], S.H. Zhu [bq], T.J. Zhu [bx], W.J. Zhu [al], Y.C. Zhu [br,ay,az], Z.A. Zhu [a,bf], B.S. Zou [a], J.H. Zou [a]

[a] Institute of High Energy Physics, Beijing 100049, People's Republic of China
[b] Beihang University, Beijing 100191, People's Republic of China
[c] Beijing Institute of Petrochemical Technology, Beijing 102617, People's Republic of China
[d] Bochum Ruhr-University, D-44780 Bochum, Germany
[e] Carnegie Mellon University, Pittsburgh, PA 15213, USA
[f] Central China Normal University, Wuhan 430079, People's Republic of China
[g] China Center of Advanced Science and Technology, Beijing 100190, People's Republic of China
[h] COMSATS University Islamabad, Lahore Campus, Defence Road, Off Raiwind Road, 54000 Lahore, Pakistan
[i] Fudan University, Shanghai 200443, People's Republic of China
[j] G.I. Budker Institute of Nuclear Physics SB RAS (BINP), Novosibirsk 630090, Russia
[k] GSI Helmholtzcentre for Heavy Ion Research GmbH, D-64291 Darmstadt, Germany
[l] Guangxi Normal University, Guilin 541004, People's Republic of China
[m] Guangxi University, Nanning 530004, People's Republic of China
[n] Hangzhou Normal University, Hangzhou 310036, People's Republic of China
[o] Helmholtz Institute Mainz, Johann-Joachim-Becher-Weg 45, D-55099 Mainz, Germany
[p] Henan Normal University, Xinxiang 453007, People's Republic of China
[q] Henan University of Science and Technology, Luoyang 471003, People's Republic of China
[r] Huangshan College, Huangshan 245000, People's Republic of China
[s] Hunan Normal University, Changsha 410081, People's Republic of China
[t] Hunan University, Changsha 410082, People's Republic of China
[u] Indian Institute of Technology Madras, Chennai 600036, India
[v] Indiana University, Bloomington, IN 47405, USA
[w] INFN Laboratori Nazionali di Frascati, I-00044, Frascati, Italy
[x] INFN Sezione di Ferrara, I-44122, Ferrara, Italy
[y] INFN Sezione di Perugia, I-06100, Perugia, Italy
[z] INFN Sezione di Torino, I-10125, Turin, Italy
[aa] Institute of Modern Physics, Lanzhou 730000, People's Republic of China
[ab] Institute of Physics and Technology, Peace Ave. 54B, Ulaanbaatar 13330, Mongolia
[ac] Jilin University, Changchun 130012, People's Republic of China
[ad] Johannes Gutenberg University of Mainz, Johann-Joachim-Becher-Weg 45, D-55099 Mainz, Germany
[ae] Joint Institute for Nuclear Research, 141980 Dubna, Moscow region, Russia
[af] Justus-Liebig-Universitaet Giessen, II. Physikalisches Institut, Heinrich-Buff-Ring 16, D-35392 Giessen, Germany
[ag] Lanzhou University, Lanzhou 730000, People's Republic of China
[ah] Liaoning Normal University, Dalian 116029, People's Republic of China
[ai] Liaoning University, Shenyang 110036, People's Republic of China
[aj] Nanjing Normal University, Nanjing 210023, People's Republic of China
[ak] Nanjing University, Nanjing 210093, People's Republic of China
[al] Nankai University, Tianjin 300071, People's Republic of China
[am] North China Electric Power University, Beijing 102206, People's Republic of China
[an] Peking University, Beijing 100871, People's Republic of China
[ao] Qufu Normal University, Qufu 273165, People's Republic of China
[ap] Shandong Normal University, Jinan 250014, People's Republic of China
[aq] Shandong University, Jinan 250100, People's Republic of China
[ar] Shanghai Jiao Tong University, Shanghai 200240, People's Republic of China
[as] Shanxi Normal University, Linfen 041004, People's Republic of China
[at] Shanxi University, Taiyuan 030006, People's Republic of China
[au] Sichuan University, Chengdu 610064, People's Republic of China
[av] Soochow University, Suzhou 215006, People's Republic of China
[aw] South China Normal University, Guangzhou 510006, People's Republic of China
[ax] Southeast University, Nanjing 211100, People's Republic of China
[ay] State Key Laboratory of Particle Detection and Electronics, Beijing 100049, People's Republic of China
[az] State Key Laboratory of Particle Detection and Electronics, Hefei 230026, People's Republic of China
[ba] Sun Yat-Sen University, Guangzhou 510275, People's Republic of China
[bb] Suranaree University of Technology, University Avenue 111, Nakhon Ratchasima 30000, Thailand
[bc] Tsinghua University, Beijing 100084, People's Republic of China
[bd] Turkish Accelerator Center Particle Factory Group, Istanbul Bilgi University, 34060 Eyup, Istanbul, Turkey
[be] Turkish Accelerator Center Particle Factory Group, Near East University, Nicosia, North Cyprus, Mersin 10, Turkey
[bf] University of Chinese Academy of Sciences, Beijing 100049, People's Republic of China
[bg] University of Eastern Piedmont, I-15121, Alessandria, Italy
[bh] University of Ferrara, I-44122, Ferrara, Italy
[bi] University of Groningen, NL-9747 AA Groningen, the Netherlands
[bj] University of Hawaii, Honolulu, HI 96822, USA
[bk] University of Jinan, Jinan 250022, People's Republic of China
[bl] University of Manchester, Oxford Road, Manchester, M13 9PL, United Kingdom
[bm] University of Minnesota, Minneapolis, MN 55455, USA
[bn] University of Muenster, Wilhelm-Klemm-Str. 9, 48149 Muenster, Germany
[bo] University of Perugia, I-06100, Perugia, Italy
[bp] University of Oxford, Keble Rd, Oxford, OX13RH, United Kingdom
[bq] University of Science and Technology Liaoning, Anshan 114051, People's Republic of China
[br] University of Science and Technology of China, Hefei 230026, People's Republic of China
[bs] University of South China, Hengyang 421001, People's Republic of China
[bt] University of the Punjab, Lahore-54590, Pakistan
[bu] University of Turin, INFN, I-10125, Turin, Italy
[bv] Uppsala University, Box 516, SE-75120 Uppsala, Sweden
[bw] Wuhan University, Wuhan 430072, People's Republic of China
[bx] Xinyang Normal University, Xinyang 464000, People's Republic of China

[by] Zhejiang University, Hangzhou 310027, People's Republic of China
[bz] Zhengzhou University, Zhengzhou 450001, People's Republic of China

ARTICLE INFO

Article history:
Received 14 September 2020
Received in revised form 6 November 2020
Accepted 23 November 2020
Available online 8 December 2020
Editor: M. Doser

Keywords:
Hadronic cross section
Muon anomaly
Initial state radiation
Pion form factor
Covariance matrix
BESIII

ABSTRACT

In Ref. [1] the BESIII collaboration published a cross section measurement of the process $e^+e^- \to \pi^+\pi^-$ in the energy range between 600 and 900 MeV. In this corrigendum, we report a corrected evaluation of the statistical errors in terms of a fully propagated covariance matrix. The correction also yields a reduced statistical uncertainty for the hadronic vacuum polarization contribution to the anomalous magnetic moment of the muon, which now reads as $a_\mu^{\pi\pi,\mathrm{LO}}(600-900\ \mathrm{MeV}) = (368.2 \pm 1.5_{\mathrm{stat}} \pm 3.3_{\mathrm{syst}}) \times 10^{-10}$. The central values of the cross section measurement and of $a_\mu^{\pi\pi,\mathrm{LO}}$, as well as the systematic uncertainties remain unchanged.

1. Introduction

Previously, we reported [1] a measurement of the cross section $\sigma^{\mathrm{bare}}(e^+e^- \to \pi^+\pi^-)$ and the pion form factor $|F_\pi|^2$ in the energy range between 600 MeV and 900 MeV. As pointed out in Refs. [2] and [3], there exists a difference between the statistical uncertainties of the tabulated cross section of Ref. [1] and the covariance matrix, which is documented as a supplemental material to the publication. Furthermore, when including the covariance matrix, it is not possible to reproduce the fit of the form factor presented in Ref. [1].

In scrutinizing the published analysis, we realized that the covariance matrix had been provided at the level of the event yield, not, as claimed, at the level of the cross section. The same matrix is erroneously used in the calculation of $a_\mu^{\pi\pi,\mathrm{LO}}$. At the same time, the statistical errors in Tab. 4 of Ref. [1] are taken from the event yield prior to unfolding and are propagated to the level of the cross section and form factor, respectively, producing two different statistical uncertainties for the results.

In this work, the statistical uncertainties are reevaluated and an updated value of the uncertainty of the two-pion contribution to the hadronic vacuum polarization contribution of the anomalous magnetic moment of the muon, $a_\mu^{\pi\pi,\mathrm{LO}}$, is calculated.

2. Reevaluation of the statistical covariance matrix

The covariance matrix results from the unfolding procedure, which is applied at the level of the event yield to compensate for mass resolution effects of the detector. The underlying algorithm of the procedure is based on singular value decomposition [4]. The covariance matrix needs to be propagated according to generalized Gaussian error propagation to correctly reflect the statistical correlations of the cross section and the form factor, respectively.

In an initial state radiation (ISR) measurement, the dressed cross section $\sigma^{\mathrm{dressed}}(e^+e^- \to \pi^+\pi^-)$ is calculated from the unfolded event yield N_{unf} of $\pi^+\pi^-\gamma_{\mathrm{ISR}}$ events according to

$$\sigma^{\mathrm{dressed}}(e^+e^- \to \pi^+\pi^-) = \frac{N_{\mathrm{unf}}}{\varepsilon^{\pi\pi}_{\mathrm{global}} \cdot \mathcal{L}_{\mathrm{int}} \cdot H(s,s') \cdot (1+\delta^{\pi\pi\gamma}_{\mathrm{FSR}})}, \tag{1}$$

where $\varepsilon^{\pi\pi}_{\mathrm{global}}$ is the reconstruction efficiency, $\mathcal{L}_{\mathrm{int}}$ is the integrated luminosity, and $H(s,s')$ is the radiator function, where the implementation of Ref. [5] is considered. The correction $(1+\delta^{\pi\pi\gamma}_{\mathrm{FSR}})$ denotes the final state radiation (FSR) corrections on the level of radiative $\pi^+\pi^-\gamma$ events.[14]

The *bare* cross section is obtained from the dressed cross section by applying mass-dependent corrections for vacuum polarization δ_{VP} [6] and by adding back effects of FSR on the level of the non-radiative $\pi^+\pi^-$ cross sections as parametrized within scalar QED in the Schwinger term $1+\eta(s')\frac{\alpha}{\pi}$ [7]. The final formula for the bare cross section reads as:

$$\sigma^{\mathrm{bare}}(e^+e^- \to \pi^+\pi^-(\gamma_{\mathrm{FSR}})) = \sigma^{\mathrm{dressed}}(e^+e^- \to \pi^+\pi^-)\frac{1+\eta(s')\frac{\alpha}{\pi}}{\delta_{\mathrm{VP}}(s')}, \tag{2}$$

where s' denotes the two-pion invariant mass squared.

Since all the above mentioned values remain unchanged compared to the original work [1], the central value of the cross section does not change.

The covariance matrix obtained from the unfolding procedure is propagated taking into account Eqs. (1) and (2) to the level of the bare cross section. It is, assuming no correlations between the contributing quantities, thus, given by

$$C^{\sigma^{\mathrm{bare}}} = \sum_{k\in\{N,\varepsilon,\mathcal{L}_{\mathrm{int}},H,(1+\delta^{\pi\pi\gamma}_{\mathrm{FSR}})\}} \left(J^{\mathrm{T}}\right)^k C^k J^k, \tag{3}$$

with $J^k_{ij} = \frac{\partial \sigma^{\mathrm{bare}}_i}{\partial k_j}$ being the Jacobian matrix of the bare cross section with respect to the contribution k to the statistical uncertainty, according to generalized Gaussian error propagation.

Since the time integrated luminosity is a single scalar value, its covariance matrix is simply given by the squared statistical uncertainty of the time integrated luminosity: $C^{\mathcal{L}_{\mathrm{int}}} = (\Delta\mathcal{L}_{\mathrm{int}})^2$.

It is assumed that the reconstruction efficiency, the time integrated luminosity, the radiator function, as well as the final state radiation correction term are completely uncorrelated. The respective diagonal elements of the covariance matrices are given by the square of the uncertainties. The contribution of the Schwinger correction term is neglected, since as a QED calculation, it is assumed to be exact. In the original work, the uncertainty of the vacuum polarization effect is considered to be purely systematic. Hence, it

[14] In Eq. (1) of Ref. [1], the factor $(1+\delta^{\pi\pi}_{\mathrm{FSR}})$ should be read as $\left[\frac{1+\eta(s)\frac{\alpha}{\pi}}{1+\delta^{\pi\pi\gamma}_{\mathrm{FSR}}}\right]$, contrary to the description in Section 6.3 therein.

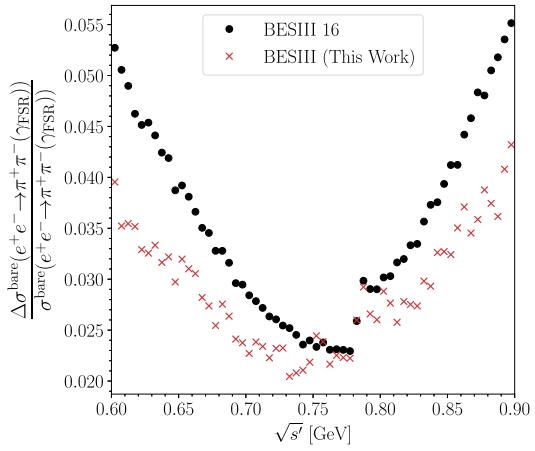

Fig. 1. Relative uncertainty of the bare cross section $\sigma^{\text{bare}}(e^+e^+ \to \pi^+\pi^-(\gamma_{\text{FSR}}))$ of this work (red crosses) compared to the results of Ref. [1] (black circles). The uncertainties of the cross section of this work are the square roots of the diagonal elements of the matrix.

is also neglected in the calculation of the statistical covariance matrix.

In the original publication, the error propagation of the covariance matrix had not been carried out properly. As a result, the statistical uncertainties of the published cross section do not reflect the information of the unfolding. Fig. 1 shows a comparison of the relative statistical errors of the bare cross sections calculated as the diagonal uncertainties of this work (red crosses) and the uncertainties published in Ref. [1] (black circles). The values of the diagonal errors are listed in Table 1.

It must be stressed that only the statistical uncertainties of the measurements of $\sigma^{\text{bare}}(e^+e^+ \to \pi^+\pi^-(\gamma_{\text{FSR}}))$ and of $|F_\pi|^2$ have been reevaluated. Thus, the systematic uncertainty of 0.9% evaluated in Ref. [1] is unchanged.

The BESIII collaboration has approved new data taking at 3.773 GeV in 2021-2022, aiming at a total data set of 20 fb^{-1} [8]. In addition to a significant reduction of the statistical uncertainty, the new data will also allow for the alternative normalization scheme for $\sigma^{\text{bare}}(e^+e^+ \to \pi^+\pi^-(\gamma_{\text{FSR}}))$, discussed in Eq. (3) of Ref. [1], in which the dominating systematic uncertainties cancel. A total uncertainty of 0.6% can be expected.

3. Gounaris-Sakurai fit of the pion form factor

The pion form factor $|F_\pi|^2$ is defined as

$$|F_\pi|^2 = \frac{3s'}{\pi\alpha\beta_\pi^3(s')} \cdot \sigma^{\text{dressed}}(e^+e^- \to \pi^+\pi^-)\,, \tag{4}$$

where $\beta_\pi = \sqrt{1-4m_\pi^2/s'}$ denotes the pion velocity. The factor $\frac{3s'}{\pi\alpha\beta_\pi^3(s')}$ from pure QED calculations is considered to be exact. Thus, the statistical error-covariance matrix of the pion form factor is constructed analogously to Eq. (3) from the covariance matrix of the event yield, which is propagated according to Eqs. (1) and (4) to the level of the form factor. The diagonal elements of the matrix are presented as updated statistical uncertainties of the pion form factor in Table 1.

In the original work, a fit of the Gounaris-Sakurai parametrization [9] to the pion form factor is used to compare the BESIII measurement to previous publications. In the fit, the statistical covariance matrix is not considered. Instead, the uncertainties before having applied the unfolding procedure are considered. These are assumed to implicitly take into account all correlations. A good fit quality is achieved, but cannot be reproduced using the originally published covariance matrix in Ref. [2].

In this corrigendum, we repeat the fit of the form factor as a cross check of the newly derived covariance matrix. In order to evaluate the effects of the different treatment of the statistical errors, the width of the ω meson Γ_ω is fixed to the PDG

Table 1
Results for the bare cross section $\sigma^{\text{bare}}_{\pi^+\pi^-}$ and the pion form factor together with their statistical uncertainties. The systematical uncertainties are given by 0.9% [1].

$\sqrt{s'}$ [MeV]	$\sigma^{\text{bare}}_{\pi^+\pi^-(\gamma_{\text{FSR}})}$ [nb]	$\lvert F_\pi\rvert^2$	$\sqrt{s'}$ [MeV]	$\sigma^{\text{bare}}_{\pi^+\pi^-(\gamma_{\text{FSR}})}$	$\lvert F_\pi\rvert^2$
602.5	288.3 ± 11.4	6.9 ± 0.3	752.5	1276.1 ± 31.2	41.8 ± 1.0
607.5	306.6 ± 10.8	7.4 ± 0.3	757.5	1315.9 ± 31.4	43.6 ± 1.0
612.5	332.8 ± 11.8	8.2 ± 0.3	762.5	1339.3 ± 29.0	44.8 ± 1.0
617.5	352.5 ± 12.4	8.7 ± 0.3	767.5	1331.9 ± 30.0	45.0 ± 1.0
622.5	367.7 ± 12.1	9.2 ± 0.3	772.5	1327.0 ± 29.6	45.2 ± 1.0
627.5	390.1 ± 12.7	9.8 ± 0.3	777.5	1272.7 ± 28.3	43.7 ± 1.0
632.5	408.0 ± 13.6	10.4 ± 0.3	782.5	1031.5 ± 26.8	37.1 ± 1.0
637.5	426.6 ± 13.5	11.0 ± 0.3	787.5	810.7 ± 23.7	30.3 ± 0.9
642.5	453.5 ± 14.6	11.8 ± 0.4	792.5	819.7 ± 21.8	30.6 ± 0.8
647.5	477.7 ± 14.2	12.5 ± 0.4	797.5	803.1 ± 20.9	30.1 ± 0.8
652.5	497.4 ± 15.9	13.2 ± 0.4	802.5	732.4 ± 21.1	27.7 ± 0.8
657.5	509.2 ± 15.8	13.6 ± 0.4	807.5	679.9 ± 18.8	25.9 ± 0.7
662.5	543.4 ± 16.6	14.7 ± 0.4	812.5	663.6 ± 17.1	25.5 ± 0.7
667.5	585.0 ± 16.5	16.0 ± 0.4	817.5	622.2 ± 17.3	24.1 ± 0.7
672.5	642.7 ± 17.6	17.7 ± 0.5	822.5	585.0 ± 16.1	22.9 ± 0.6
677.5	640.5 ± 16.3	17.8 ± 0.5	827.5	540.8 ± 14.8	21.4 ± 0.6
682.5	668.0 ± 18.4	18.8 ± 0.5	832.5	496.4 ± 14.8	19.8 ± 0.6
687.5	724.4 ± 19.1	20.6 ± 0.5	837.5	450.4 ± 13.2	18.1 ± 0.5
692.5	783.5 ± 18.9	22.5 ± 0.5	842.5	404.7 ± 13.2	16.4 ± 0.5
697.5	858.6 ± 20.4	24.9 ± 0.6	847.5	391.3 ± 12.8	16.0 ± 0.5
702.5	893.8 ± 20.3	26.2 ± 0.6	852.5	364.0 ± 11.8	15.0 ± 0.5
707.5	897.8 ± 21.4	26.6 ± 0.6	857.5	339.6 ± 11.9	14.2 ± 0.5
712.5	978.6 ± 22.9	29.3 ± 0.7	862.5	310.0 ± 11.5	13.0 ± 0.5
717.5	1059.1 ± 23.6	32.0 ± 0.7	867.5	283.8 ± 9.8	12.1 ± 0.4
722.5	1086.0 ± 25.2	33.2 ± 0.8	872.5	256.5 ± 9.2	11.0 ± 0.4
727.5	1088.4 ± 25.3	33.6 ± 0.8	877.5	237.3 ± 9.2	10.3 ± 0.4
732.5	1158.8 ± 23.7	36.2 ± 0.7	882.5	229.7 ± 8.6	10.0 ± 0.4
737.5	1206.5 ± 25.1	38.2 ± 0.8	887.5	224.0 ± 8.1	9.9 ± 0.4
742.5	1229.9 ± 25.9	39.3 ± 0.8	892.5	196.1 ± 8.0	8.7 ± 0.4
747.5	1263.3 ± 27.6	40.9 ± 0.9	897.5	175.9 ± 7.6	7.9 ± 0.3

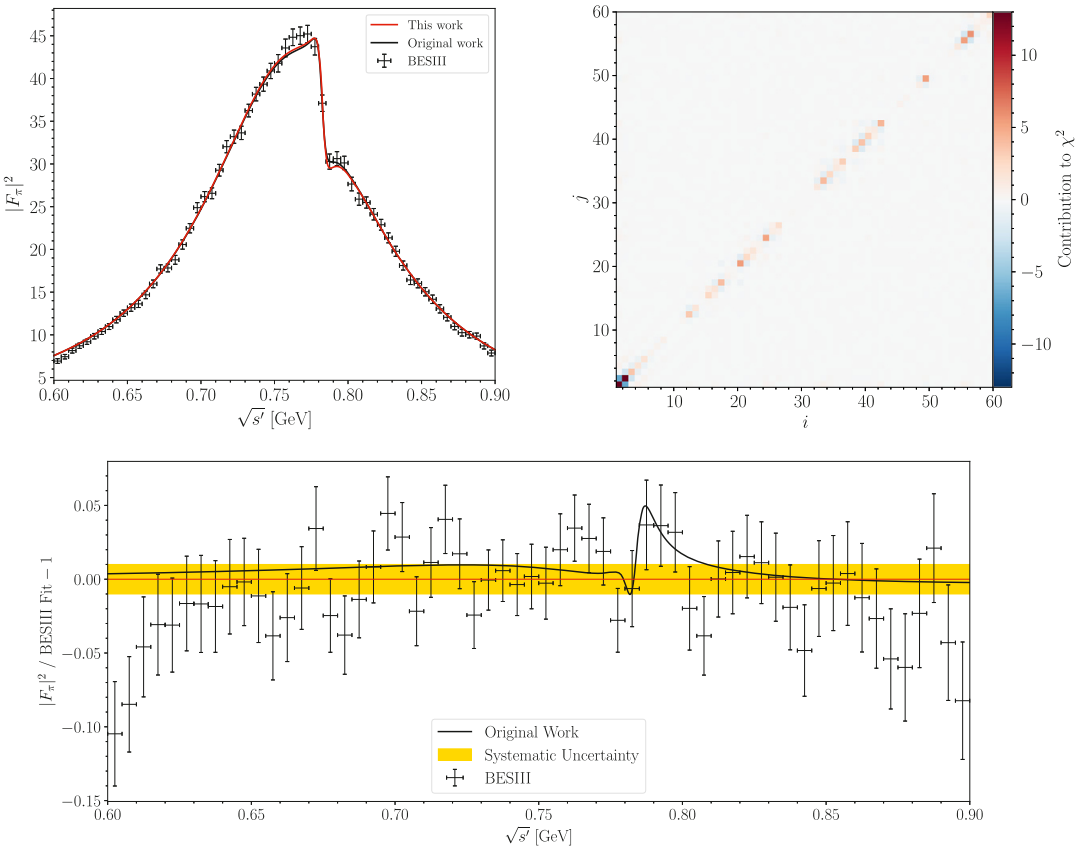

Fig. 2. Top Left: Results of the Gounaris-Sakurai fit of the original work [1] (black) and this work (red); **Top Right:** Contribution to the χ^2 value of the individual bins of the covariance matrix; **Bottom:** Deviations between the fit result of this work (red line) and the data as well as the old fit [1] (black line).

Table 2
Fit results together with the statistical uncertainties from this work (BESIII), the original work (BESIII 16 [1]), the BaBar measurement [11], and the PDG values [10].

Parameter	BESIII	BESIII 16	BaBar	PDG
m_ρ [MeV]	776.58 ± 0.42	776.0 ± 0.4	775.02 ± 0.31	775.26 ± 0.25
Γ_ρ [MeV]	152.05 ± 0.65	151.7 ± 0.7	149.59 ± 0.67	147.8 ± 0.9
m_ω [MeV]	782.69 ± 0.34	782.2 ± 0.6	781.91 ± 0.18	782.65 ± 0.12
$\lvert c_\omega \rvert$ [10^{-3}]	1.92 ± 0.16	1.7 ± 0.2	1.644 ± 0.061	–
ϕ_ω [rad]	0.15 ± 0.11	0.04 ± 0.13	-0.011 ± 0.037	–
χ^2/n.d.f.	70.70/56	49.1/56	–	–

value [10], and the masses and widths of the higher ρ states $\rho(1450)$, $\rho(1700)$, and $\rho(2150)$ are fixed to the values obtained by the BaBar collaboration [11], as done in the original work. The updated fit result is illustrated with a red line in the top left panel of Fig. 2 and compared to the original fit result. The updated fit yields a reduced χ^2 value of $\chi^2/\text{n.d.f.} = 70.70/56$. The bottom panel of Fig. 2 illustrates the deviations of the updated fit result and the old fit result from Ref. [1]. A clear deviation is found at the $\rho-\omega$ interference, where using the covariance matrix in the fit has worsened the agreement with data. The effect is related to fixing Γ_ω in the fit. However, floating the width does not only result in a better agreement between data and fit function, but also in a value of Γ_ω more than two standard deviations larger than the PDG value. The top right panel of Fig. 2 shows the individual contributions of the bins of the covariance matrix to the total χ^2 value. Large fluctuations, as reported by Colangelo et al. [2] are not observed. The largest contribution to χ^2 stems from the mass region between 600 and 615 MeV, where there is a systematic difference between the data and the Gounaris-Sakurai parametrization. The fit results are summarized in Table 2.

By comparing the resulting parameters one finds a significant improvement of the uncertainty of the ω mass. The results obtained for other parameters agree well with the original work. Thus, the systematic differences found between the BESIII result and previous measurements using the Gounaris-Sakurai fit in Ref. [1] can be considered unchanged. The deviations between the fit results of BESIII and BaBar are on the level of 3σ or less, which might be well covered by systematic effects that are neglected at this point. It should also be noted that the BaBar results do not consider the covariance matrix in the fit due to expected biases [11]. The precise determination of resonance parameters is not the purpose of this corrigendum.

4. Reevaluation of $a_\mu^{\pi\pi,\text{LO}}$(600 – 900 MeV)

The hadronic vacuum polarization (HVP) contribution to the muon anomalous magnetic moment a_μ can be connected to the cross section $\sigma(e^+e^- \to \text{hadrons})$ using the optical theorem [12]. The contribution of $e^+e^- \to \pi^+\pi^-$ to a_μ in the mass range of the ρ–ω interference is given by

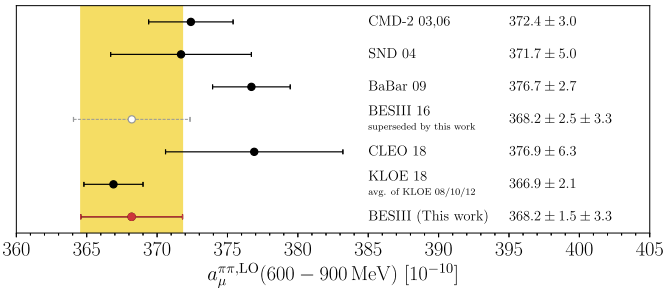

Fig. 3. Comparison of the updated calculation of the leading-order (LO) hadronic vacuum polarization contribution to $(g-2)_\mu$ due to $\pi^+\pi^-$ in the energy range 600 - 900 MeV from BESIII and the corresponding results from CMD-2 [13,14], SND [15], BaBar [11], BESIII 16 [1], CLEO [16], and KLOE [17]. The respective values are taken from the white paper of the *Muon g-2 Theory Initiative* [2,3,18–22]. The yellow band indicates the 1σ range of the updated BESIII result.

$$a_\mu^{\pi\pi,\mathrm{LO}}(600-900\ \mathrm{MeV}) = \frac{1}{4\pi^3}\int_{(600\ \mathrm{MeV})^2}^{(900\ \mathrm{MeV})^2} \mathrm{d}s'\, K(s')\,\sigma^{\mathrm{bare}}(e^+e^-\to\pi^+\pi^-(\gamma_{\mathrm{FSR}}))\,, \quad (5)$$

where $K(s')$ is a kernel function.

With the systematical uncertainty remaining at 0.9% [1], the BESIII result on the hadronic vacuum polarization now reads as $a_\mu^{\pi\pi,\mathrm{LO}}(600-900\ \mathrm{MeV}) = (368.2 \pm 1.5_{\mathrm{stat}} \pm 3.3_{\mathrm{syst}}) \times 10^{-10}$.

Fig. 3 shows the results of the calculation compared to previous measurements. The statistical uncertainty is reduced by 40% compared to the original work. The result lines up well with the KLOE results, while the 1.7σ discrepancy between the BESIII and BaBar results remains.

Declaration of competing interest

The authors declare that they have no known competing financial interests or personal relationships that could have appeared to influence the work reported in this paper.

Acknowledgements

The BESIII collaboration thanks the staff of BEPCII and the IHEP computing center for their strong support. This work is supported in part by National Key Basic Research Program of China under Contract No. 2015CB856700; National Natural Science Foundation of China (NSFC) under Contracts Nos. 11625523, 11635010, 11735014, 11822506, 11835012, 11935015, 11935016, 11935018, 11961141012; the Chinese Academy of Sciences (CAS) Large-Scale Scientific Facility Program; Joint Large-Scale Scientific Facility Funds of the NSFC and CAS under Contracts Nos. U1732263, U1832207; CAS Key Research Program of Frontier Sciences under Contracts Nos. QYZDJ-SSW-SLH003, QYZDJ-SSW-SLH040; 100 Talents Program of CAS; INPAC and Shanghai Key Laboratory for Particle Physics and Cosmology; ERC under Contract No. 758462; German Research Foundation DFG under Contracts Nos. 443159800, Collaborative Research Center CRC 1044, FOR 2359, FOR 2359, GRK 214; Istituto Nazionale di Fisica Nucleare, Italy; Ministry of Development of Turkey under Contract No. DPT2006K-120470; National Science and Technology fund; Olle Engkvist Foundation under Contract No. 200-0605; STFC (United Kingdom); The Knut and Alice Wallenberg Foundation (Sweden) under Contract No. 2016.0157; The Royal Society, UK under Contracts Nos. DH140054, DH160214; The Swedish Research Council; U.S. Department of Energy under Contracts Nos. DE-FG02-05ER41374, DE-SC-0012069.

Appendix A. Supplementary material

Supplementary material related to this article can be found online at https://doi.org/10.1016/j.physletb.2020.135982.

References

[1] M. Ablikim, et al., Measurement of the $e^+e^-\to\pi^+\pi^-$ cross section between 600 and 900 MeV using initial state radiation, Phys. Lett. B 753 (2016) 629–638, https://doi.org/10.1016/j.physletb.2015.11.043, arXiv:1507.08188.

[2] G. Colangelo, M. Hoferichter, P. Stoffer, Two-pion contribution to hadronic vacuum polarization, J. High Energy Phys. 02 (2019) 006, https://doi.org/10.1007/JHEP02(2019)006, arXiv:1810.00007.

[3] M. Davier, A. Hoecker, B. Malaescu, Z. Zhang, A new evaluation of the hadronic vacuum polarisation contributions to the muon anomalous magnetic moment and to $\alpha(m_Z^2)$, Eur. Phys. J. C 80 (3) (2020) 241, https://doi.org/10.1140/epjc/s10052-020-7792-2, arXiv:1908.00921.

[4] A. Hocker, V. Kartvelishvili, SVD approach to data unfolding, Nucl. Instrum. Methods A 372 (1996) 469–481, https://doi.org/10.1016/0168-9002(95)01478-0, arXiv:hep-ph/9509307.

[5] G. Rodrigo, H. Czyz, J.H. Kuhn, M. Szopa, Radiative return at NLO and the measurement of the hadronic cross-section in electron positron annihilation, Eur. Phys. J. C 24 (2002) 71–82, https://doi.org/10.1007/s100520200912, arXiv:hep-ph/0112184.

[6] F. Jegerlehner, Hadronic contributions to electroweak parameter shifts: a detailed analysis, Z. Phys. C 32 (1986) 195, https://doi.org/10.1007/BF01552495, www-com.physik.hu-berlin.de/~fjeger/alphaQED.tar.gz, 2015.

[7] J.S. Schwinger, Particles, Sources, and Fields, vol. 3, Perseus, 1989.

[8] M. Ablikim, et al., Future physics programme of BESIII, Chin. Phys. C 44 (4) (2020) 040001, https://doi.org/10.1088/1674-1137/44/4/040001, arXiv:1912.05983.

[9] G. Gounaris, J. Sakurai, Finite width corrections to the vector meson dominance prediction for $\rho\to e^+e^-$, Phys. Rev. Lett. 21 (1968) 244–247, https://doi.org/10.1103/PhysRevLett.21.244.

[10] P. Zyla, et al., Rev. Part. Phys., PTEP 2020 (8) (2020) 083C01, https://doi.org/10.1093/ptep/ptaa104.

[11] J.P. Lees, et al., Precise measurement of the $e^+e^-\to\pi^+\pi^-(\gamma)$ cross section with the initial-state radiation method at BABAR, Phys. Rev. D 86 (2012) 032013, https://doi.org/10.1103/PhysRevD.86.032013, arXiv:1205.2228.

[12] S. Eidelman, F. Jegerlehner, Hadronic contributions to (g-2) of the leptons and to the effective fine structure constant alpha (M_Z^2), Z. Phys. C 67 (1995) 585–602, https://doi.org/10.1007/BF01553984, arXiv:hep-ph/9502298.

[13] R.R. Akhmetshin, et al., Reanalysis of hadronic cross-section measurements at CMD-2, Phys. Lett. B 578 (2004) 285–289, https://doi.org/10.1016/j.physletb.2003.10.108, arXiv:hep-ex/0308008.

[14] R.R. Akhmetshin, et al., High-statistics measurement of the pion form factor in the rho-meson energy range with the CMD-2 detector, Phys. Lett. B 648 (2007) 28–38, https://doi.org/10.1016/j.physletb.2007.01.073, arXiv:hep-ex/0610021.

[15] M.N. Achasov, et al., Update of the $e^+e^-\to\pi^+\pi^-$ cross-section measured by SND detector in the energy region 400 MeV $<\sqrt{s}<$ 1000 MeV, J. Exp. Theor. Phys. 103 (2006) 380–384, https://doi.org/10.1134/S106377610609007X; Zh. Eksp. Teor. Fiz. 130 (2006) 437, arXiv:hep-ex/0605013.

[16] T. Xiao, S. Dobbs, A. Tomaradze, K.K. Seth, G. Bonvicini, Precision measurement of the hadronic contribution to the muon anomalous magnetic moment, Phys. Rev. D 97 (3) (2018) 032012, https://doi.org/10.1103/PhysRevD.97.032012, arXiv:1712.04530.

[17] A. Anastasi, et al., Combination of KLOE $\sigma\left(e^+e^-\to\pi^+\pi^-\gamma(\gamma)\right)$ measurements and determination of $a_\mu^{\pi^+\pi^-}$ in the energy range $0.10<s<0.95$ GeV^2, J. High Energy Phys. 03 (2018) 173, https://doi.org/10.1007/JHEP03(2018)173, arXiv:1711.03085.

[18] T. Aoyama, et al., The anomalous magnetic moment of the muon in the standard model (6 2020), arXiv:2006.04822.

[19] M. Davier, A. Hoecker, B. Malaescu, Z. Zhang, Reevaluation of the hadronic vacuum polarisation contributions to the standard model predictions of the muon $g-2$ and $\alpha(m_Z^2)$ using newest hadronic cross-section data, Eur. Phys. J. C 77 (12) (2017) 827, https://doi.org/10.1140/epjc/s10052-017-5161-6, arXiv:1706.09436.

[20] A. Keshavarzi, D. Nomura, T. Teubner, Muon $g-2$ and $\alpha(M_Z^2)$: a new data-based analysis, Phys. Rev. D 97 (11) (2018) 114025, https://doi.org/10.1103/PhysRevD.97.114025, arXiv:1802.02995.

[21] M. Hoferichter, B.-L. Hoid, B. Kubis, Three-pion contribution to hadronic vacuum polarization, J. High Energy Phys. 08 (2019) 137, https://doi.org/10.1007/JHEP08(2019)137, arXiv:1907.01556.

[22] A. Keshavarzi, D. Nomura, T. Teubner, The $g-2$ of charged leptons, $\alpha(M_Z^2)$ and the hyperfine splitting of muonium, Phys. Rev. D 101 (2020) 014029, https://doi.org/10.1103/PhysRevD.101.014029, arXiv:1911.00367.